ELSEVIER

Ore Geology Reviews 22 (2002) 91–116

ORE GEOLOGY REVIEWS

www.elsevier.com/locate/oregeorev

Syngenetic origin for the sediment-hosted disseminated gold deposits in NW Sichuan, China: ore fabric evidence

X.X. Gu[a,*], J.M. Liu[b], O. Schulz[c], F. Vavtar[c], M.H. Zheng[d]

[a] *Institute of Geochemistry, Chinese Academy of Sciences, Guiyang 550002, PR China*
[b] *Institute of Geology and Geophysics, Chinese Academy of Sciences, Beijing 100101, PR China*
[c] *Institute of Mineralogy and Petrography, University of Innsbruck, A-6020 Innsbruck, Austria*
[d] *Chengdu University of Technology, Chengdu 610059, PR China*

Received 10 October 2001; accepted 22 August 2002

Abstract

Sediment-hosted disseminated gold deposits in NW Sichuan China have many features in common with the well-known Carlin-type deposits in the western United States. They are hosted by Middle–Upper Triassic turbidites composed of 1300–4300 m of rhythmically interbedded, slightly metamorphosed calcareous sandstone, siltstone, and slate. The ore bodies are typically layer- or lens-like in shape and generally extend parallel to the stratification of the host sedimentary rocks, with a strike length of tens to several hundreds of meters. The immediate host rocks consist mainly of calcareous slate and siltstone characterized by high contents of organic matter and diagenetic pyrite. The main primary ore minerals associated with gold mineralization include pyrite, arsenopyrite, realgar, and stibnite. Gangue minerals comprise mostly quartz, calcite and dolomite. Gold is extremely fine-grained, usually less than 1 μm, and cannot be seen with an electron microscope.

Two types of ore mineralization have been recognized in the deposits. The stratiform ores are composed of rhythmical interbeds of sulfides (e.g., pyrite, arsenopyrite, realgar, stibnite) interpreted to be authigenic and detrital quartz, quartzite, sericite, and graphite of allogenic origin. They were folded and deformed concordantly with host rocks, and grade both vertically and laterally into normal country rocks. Another type of ore forms a network of numerous gold-bearing veins and veinlets of quartz–calcite–sulfides of millimeter-, centimeter-, decimeter-, and even meter-scale in width. The network ore randomly fills fissures, microfissures, and cleavages, but still is stratabound in character. Detailed studies on ore fabrics show abundant evidence for synsedimentary origins, although subsequent diagenesis, metamorphism, tectonic deformation, and epigenetic hydrothermal activity have significantly remolded the primary fabrics. Primary fabrics are shown either by rhythmical interbeds of different mineral components parallel to the bedding, or by the change of grain size of the same minerals such as pyrite, realgar, and stibnite. The layer inhomogeneity of the stratiform ore is clarified by parallel overprints of later schistosity planes, resulting in distinct grain orientation and elongation, aggregate polarization, and undulating extinction of ore minerals, especially of mechanically and chemically extremely mobile ones, such as realgar and stibnite.

It is proposed that the stratiform ores in these Chinese deposits were most probably formed concurrently with their host Middle–Upper Triassic turbidites in submarine, hot spring environments, while the network mineralization was formed as a result of complicated processes such as diagenesis, weak metamorphism, tectonic deformation, and epigenetic

* Corresponding author.
E-mail addresses: xuexiang_gu@263.net, gxx@cdut.edu.cn (X.X. Gu).

PII: S0169-1368(02)00110-5

hydrothermal activity, responsible for the remobilization or reworking of the pre-existing stratiform ores. Geochemical data also support this genetic model.

Keywords: Ore fabric; Syngenetic origin; Sediment-hosted gold deposits; China

1. Introduction

Since the discovery of the Carlin gold deposit in the early 1960s, numerous sedimentary rock-hosted disseminated gold deposits of Carlin-type have been discovered in the western United States and elsewhere in the world (e.g., Hausen and Kerr, 1968; Wells and Mullens, 1973; Radtke et al., 1980; Radtke, 1985; Bagby and Berger, 1985; Tooker, 1985; Hausen et al., 1987). Despite their economic importance and rather lengthy history of development, a consensus on the genesis of these deposits has not been achieved. Many investigators (e.g., Radtke et al., 1974, 1980; Xu et al., 1982a; Liu and Geng, 1985; Jewell and Parry, 1987; Hofstra et al., 1988, 1991; Percival et al., 1988; Li et al., 1989; Li, 1989; Zheng, 1989; Zheng et al., 1990, 1991, 1993b, 1994; Arehart et al., 1993; Arehart, 1996; Ilchik and Barton, 1997) believe that gold was scavenged from host sedimentary rocks by meteoric hydrothermal fluids and redeposited in Late Cenozoic geothermal systems resulting from high heat flow in the upper few kilometers of the earth's crust under conditions that are similar in many aspects to present-day active geothermal systems. According to this genetic model, the deposits have been assigned to a sedimentary rock-hosted epithermal or possibly telethermal category. On the other hand, Sillitoe and Bonham (1990) argued that this geothermal model for sedimentary rock-hosted gold deposits gains little support from available radiometric age data and other geologic characteristics, which suggest that mineralization was associated with intrusive activity that preceded the Miocene initiation of basin and range extension. Neither does the model explain the apparent lack of significant sedimentary rock-hosted gold mineralization in explored geothermal systems controlled by the Late Cenozoic Basin and Range faults in the western United States. They proposed thus, an alternative genetic model, in which gold was contributed by epizonal intrusions and was precipitated as distal replacements in hydrothermal systems. In addition, some researchers argued that the origin of deposits of this type is probably much more complicated than has previously been considered (Gu, 1994a, 1996; Zheng et al., 1993a; Liu, 1994; He and Gu, 2000). Most recently, Emsbo et al. (1999) have recognized a new type of gold occurrences in the Carlin trend, north-central Nevada. These occurrences are distinct from typical Carlin-type gold ores and are interpreted to be of sedimentary exhalative (sedex) origin, because they are stratiform and predate compaction and lithification of their unaltered Devonian host rocks.

Sediment-hosted disseminated gold deposits in the People's Republic of China were first recognized in the early 1980s, and since then have become one of the most important deposit types in China (Zheng, 1989; Gu, 1994a, 1996). Most famous among them are, for example, the Yata, Banqi, Getang, Sanchahe, Geyang, and Miaolong deposits in Guizhou Province (e.g., Liu and Geng, 1985; Cunningham et al., 1988; Li et al., 1989; Liu et al., 1989; Zheng, 1989; Ashley et al., 1991; Mao, 1991; Zhang et al., 1994), the Dongbeizhai, Qiaoqiaoshang, Manaoke, Zheboshan, Tuanjie, Qiuluo, and Pulongba deposits in Sichuan Province (Zheng, 1989; Zheng et al., 1990, 1991, 1993a,b,c, 1994; Gu, 1994a, 1996; Wang, 1995), the Ertaizi and Lijiagou deposits in Shaanxi Province (Feng, 1982; Shao et al., 1982; Xu et al., 1982a; Liu and Geng, 1985; Zheng, 1989), the Shixia and Hengdong deposits in Hunan Province (Liu and Geng, 1985; Zheng, 1989), and the Jinya deposit in Guangxi Province (Li et al., 1994). These deposits have many mineralogical and geochemical characteristics that are similar to those of Carlin-type gold deposits in the western United States and elsewhere.

There have been very few descriptions of the Chinese sediment-hosted disseminated gold deposits in western literature. The purpose of this paper is to document results of a detailed ore fabric study on the

deposits of this type in northwestern Sichuan Province, China, and to present our new genetic views about these deposits.

2. Regional geologic setting

The study area is located in the northwestern Sichuan Province, including portions of Songpan, Nanping, and Ruoergai Counties, and covers about 27,000 km^2 (Fig. 1). Tectonically, it is situated in the northeastern portion of the Bayanhar–Songpan–Ganze Mesozoic fold belt, which is connected to the north with the Kunlun–Qinling Late Paleozoic accretionary fold belt, to the east with the Yangtze craton, and to the southwest separated from the remaining part of the Tethys–Himalayan tectonic domain (Gu, 1994a,b).

2.1. Sedimentary rocks

The pre-Triassic rocks are composed of the pre-Sinian metamorphosed volcanic rocks and Sinian to Paleozoic slightly metamorphosed sedimentary rocks (Fig. 2). The upward Sinian sequence, several hundreds to 2500 m thick, contains pebbly sandstone and ferroan quartzite, through varicolored slate and phyllite with sandstone, to massive dolomite and intercalating slate. The Cambrian–Devonian strata are characterized by interbedded sandstone, siltstone, slate, and phyllite with a total thickness of a few to more than 10 km, while the Lower Carboniferous to Lower Permian strata consist mainly of limestone and dolomite. The Upper Permian rocks are represented by the famous Emeishan Basalt which occurs widely in W Sichuan and consists of basalt lava, associated with tuffs and agglomerates of continental and/or marine origin. The basalt, with a typical thickness of 50–400 m and a maximum thickness of about 2000 m, is thought to be related to relaxational taphrogenesis of the western margin of the Yangtze craton in the Late Permian.

The Triassic strata are characterized by a rhythmic succession of graywackes and slates. They are widespread in the study area and can be divided into the Lower, Middle–Upper, and Upper Triassic. The Middle–Upper Triassic rocks contain tens of sedimentary rock-hosted disseminated gold deposits and prospects (Fig. 1). The petrological and geochemical characteristics of the Middle–Upper Triassic sedimentary rocks, the nature of their provenance and the type of the tectonic setting, in which they were deposited were described in detail by Gu (1994a,b) and are summarized below.

The Middle–Upper Triassic flysch sequence consists of a thick succession (up to 4300 m) of slightly metamorphosed sandstone, siltstone, and slate. It commonly shows characteristic turbidite features and can be divided into three formations and five members. From oldest to youngest are the Zagunao Formation (Lower and Upper Members), the Zhuwo Formation, and the Xinduqiao Formation (Lower and Upper Members, Table 1). The rocks are quartz-intermediate (average 55%) in composition and are characterized geochemically by their moderate $Fe_2O_3^* + MgO$, TiO_2 contents and Al_2O_3/SiO_2 ratios, moderate abundances of ferromagnesian trace elements, and moderate contents of incompatible elements such as Tl, U, Zr, Hf, and total REEs. Detrital framework modes of sandstone and geochemical data indicate that the turbidites were mainly derived from a recycled orogenic provenance characterized chiefly by sedimentary–metasedimentary rocks and granite–gneisses with a variable admixture of continental island arc volcanic components. Flysch deposition took place in a back arc basin situated between an active continental margin (the Kunlun–Qinling fold belt) and a continental island arc (the Yidun island arc).

2.2. Igneous rocks

Igneous rocks in the area are not well studied and their genetic relationship to the gold mineralization is not yet clear. The earliest igneous activity took place in Late Silurian (Caledonian event) and was dominated by the submarine eruption of basic volcanic rocks. These extrusive tuffaceous to spilitic rocks are exposed near Huanglong in the southeastern district of the study area.

The Indosinian igneous rocks occurring in the Dongbeizhai gold deposits are characterized by several dikes of diabase–porphyrite intruding both the Carboniferous argillaceous limestones and the Middle–Upper Triassic slates. The dikes are in turn cut by high-angle faults and cleavages. K–Ar age determination of an unaltered whole-rock sample gives an age of 182 Ma (Gu, 1994a).

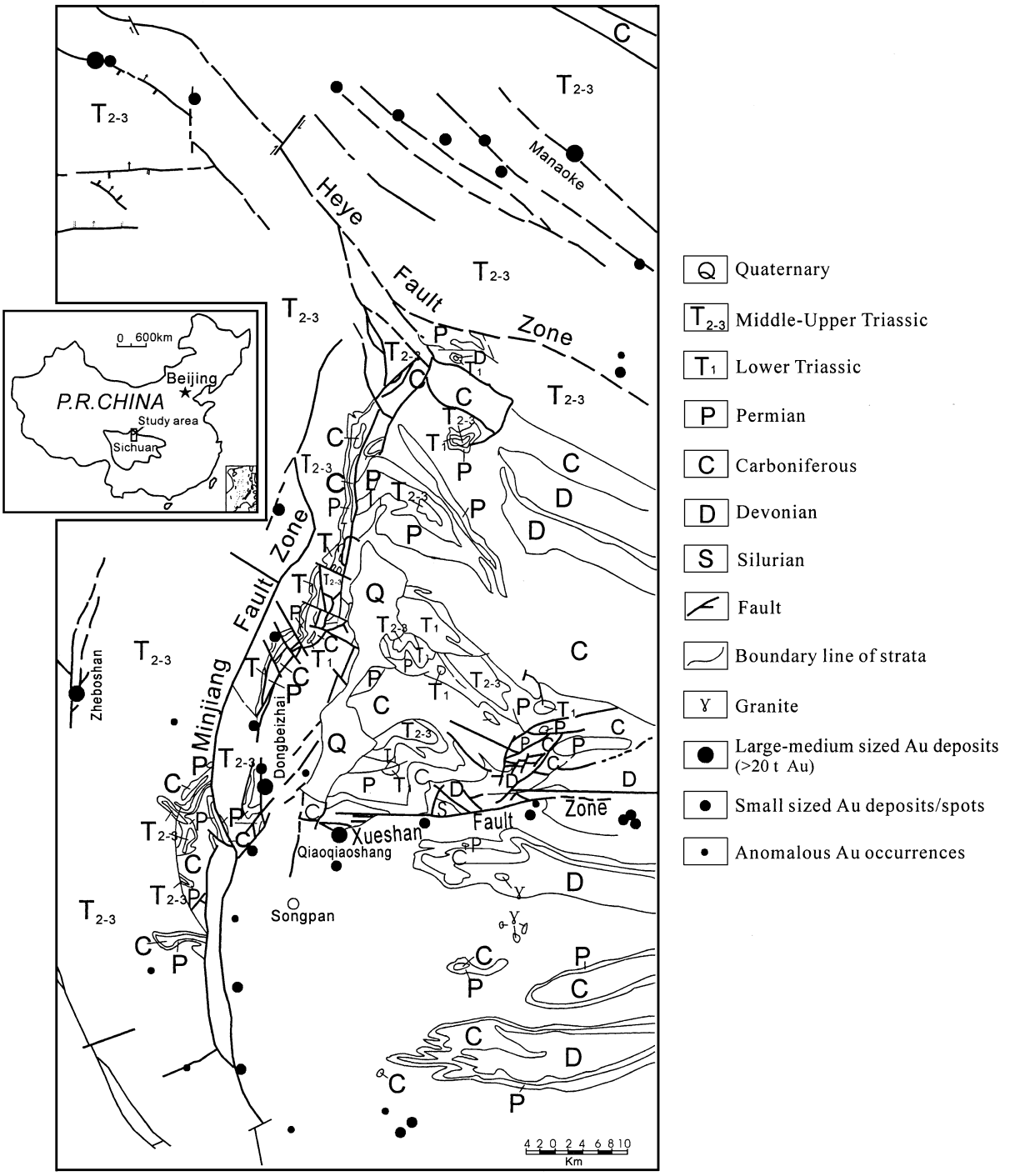

Fig. 1. Generalized geologic map of the study area (modified after Zheng et al., 1993a and Gu, 1996).

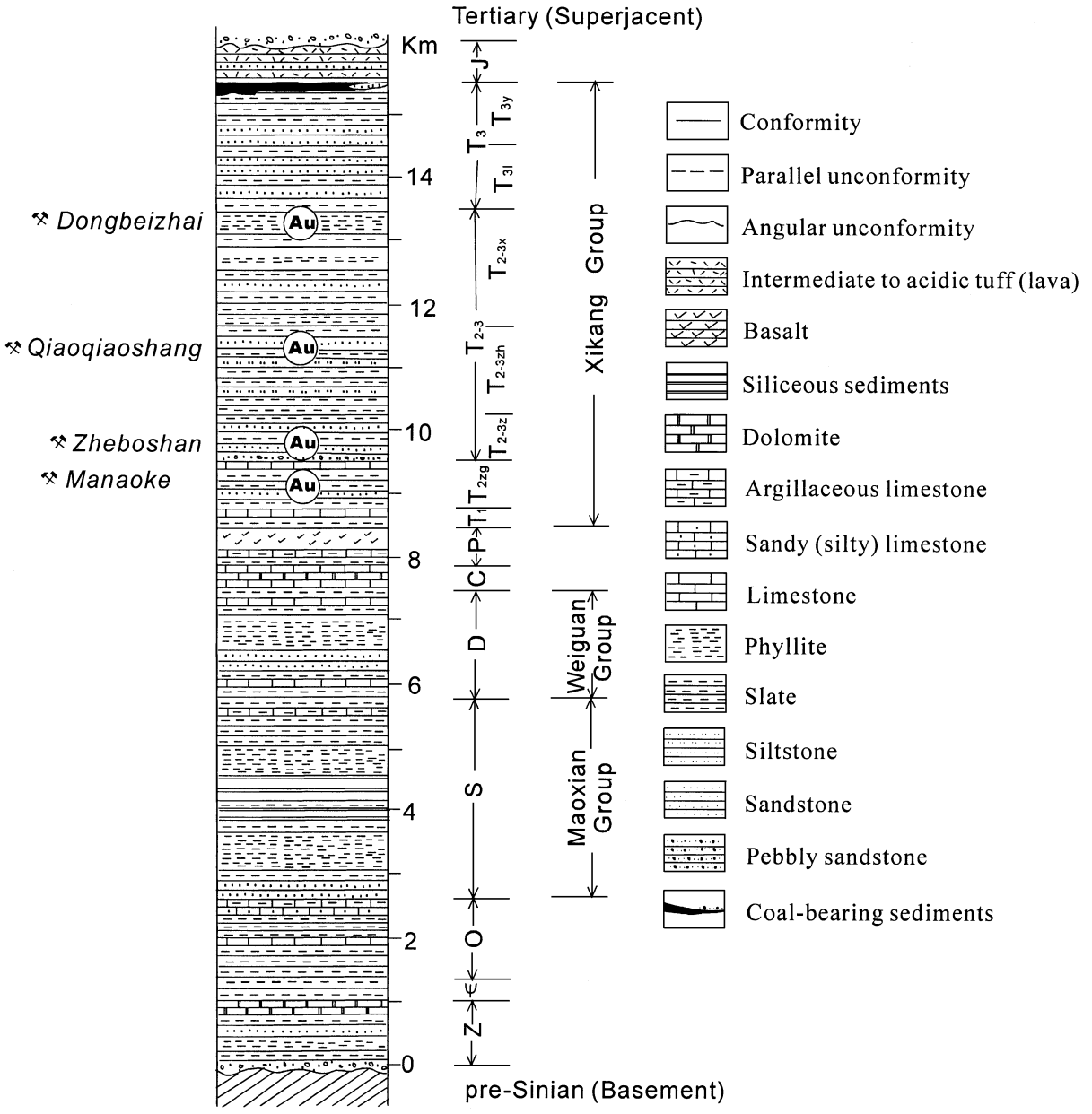

Fig. 2. Composite stratigraphic column of the study area (compiled after Xu et al., 1982b; Rao et al., 1987). Abbreviations: Z—Sinian; Є—Cambrian; O—Ordovician; S—Silurian; D—Devonian; C—Carboniferous; P—Permian; T—Triassic; J—Jurassic.

The youngest igneous activity occurred in the Qiaoqiaoshang and Zheboshan gold deposits, where dikes of quartz diorite, granodiorite, and diorite-porphyrite were emplaced along high-angle faults. K–Ar radiometric ages range from 172 to 166 Ma (Gu, 1994a).

2.3. Regional structures

The structures in the area are dominated by three groups of fault zones that dissect the district into several structural blocks (Fig. 1). They are the Min-

Table 1
Principal lithology of the Middle–Upper Triassic strata in northwestern Sichuan

Formation	Member	Thickness (m)	Lithology
Xinduqiao formation (T_{2-3x})	Upper member	100–1500	Dark gray slate interbedded with minor gray, medium- to thin-bedded, fine-grained arkosic graywacke.
	Lower member	400–800	Dark gray to black sericitic slate and carbonaceous slate interbedded with relatively minor (less than the Upper member) thin-bedded, fine-grained arkosic graywacke and siltstone. Slates contain commonly pyrites (cubic and framboidal) and locally siderite nodules.
Zhuwo formation (T_{2-3zh})		360–1000	Interbedded gray to dark gray, medium- to thick-bedded, fine-grained arkosic graywacke, silty slate, and sericitic slate with an indistinct trend of increasing-upwards sand/slate ratios.
Zagunao formation (T_{2-3z})	Upper member	400–500	Gray, thick-bedded to massive, medium- to fine-grained arkosic graywacke, and lithic feldspathic graywacke containing extremely minor dark gray sericitic slate and carbonaceous slate.
	Lower member	100–500	Gray, medium- to thin-bedded calcareous arkosic graywacke, and lithic graywacke interbedded with small amounts of dark gray sericitic slate and carbonaceous slate. Minor thin-bedded micritic limestones occur at the base of the member.

jiang N–S-trending fault zone in the west-centre, the Xueshan E–W-trending fault zone in the east, and the Heye NW–SE-trending fault zone in the north. Each fault zone is about a few to tens of kilometers wide, and tens of kilometers to more than 100 km long, and contains several subparallel major faults and subsidiary fractures. The locations of the known gold deposits and prospects seem to be controlled by these three groups of fault zones.

3. Geologic description of gold deposits

In the last decade, more than 30 stratabound disseminated gold deposits sharing many geological and geochemical characteristics have been found in the Middle–Upper Triassic sedimentary rocks in NW Sichuan. The deposits described below, Dongbeizhai, Qiaoqiaoshang, and Manaoke are most important not only for their significant reserves but also for the typical style of mineralization they have in common.

3.1. Dongbeizhai gold deposit

The Dongbeizhai deposit, the largest gold deposit yet discovered in the district, is located in Songpan County, approximately 25 km north of the town of Songpan (Fig. 1), at an elevation between 2816 and 3769 m. It was discovered as a result of a reinvestigation program of old realgar showings in the early 1980s. A detailed description of the deposit was given by Gu (1988, 1994a), Li (1989), and Zheng et al. (1993a, 1994).

Sedimentary rocks exposed in the area are Upper Paleozoic (C_3–P_1) carbonate rocks and slates interbedded with minor siltstones and sandstones of the Middle–Upper Triassic Xinduqiao Formation (T_{2-3x}, Fig. 3). The former were thrust eastward over the latter along the N–S-trending Kuashiya fault, the main structure of the deposit that has a dip of 16–35°W near surface and 67–87°W at depth. Gold mineralization is confined to a 150-m-thick section of the Xinduqiao Formation just beneath the Kuashiya fault. The immediate host rock is dark gray to black slate, interbedded with minor amounts of thin-bedded calcareous, argillaceous siltstone and sandstone. Two aspects of the fresh host-rock outline its striking petrographic characteristics: (1) the rock commonly contains 1–3% diagenetic pyrite and ca. 1% organic matter; and (2) the rock is highly shattered and deformed, especially within tens of meters from the fault plane.

The ore-bearing horizon, containing 20 stratiform ore bodies, strikes roughly north and dips west with an attitude similar to the host sedimentary rocks. The

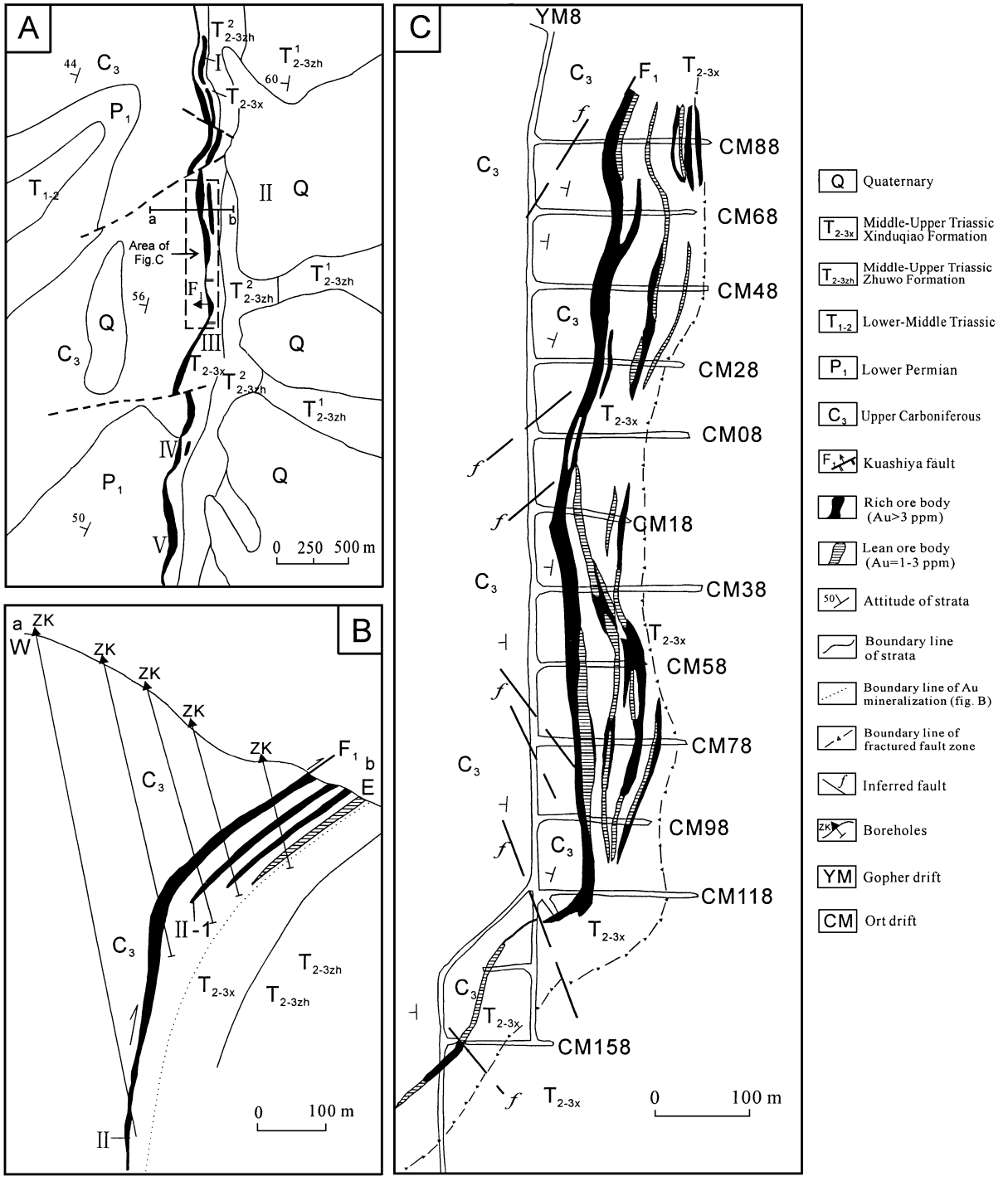

Fig. 3. (A) Simplified geologic map of the Dongbeizhai gold deposit (simplified after Li, 1989). (B) Schematic east–west cross-section based on drill holes, showing the occurrence of the ore body II in the Dongbeizhai gold deposit (after the unpublished data of the Geologic Team of NW Sichuan, 1987). (C) Geologic sketch map of the ore body II at the prospecting level of 3424 m in the Dongbeizhai gold deposit (simplified after the unpublished data of the Geologic Team of NW Sichuan, 1987).

ore bodies, with average gold grades ranging from 3 to 5 g per metric ton, are typically tabular and layer- or lens-like throughout most of their lengths. Realgar and pyrite are the most common sulfides in the deposit, although arsenopyrite, stibnite, and trace amounts of marcasite, pyrrhotite, tetrahedrite, chalcopyrite, and sphalerite are also present. Where realgar is present in the primary unoxidized ore, the boundary line of the ore body, is well defined because of the striking red to orange color of realgar. Ores without realgar closely resemble normal host rocks, thus whether or not they have been mineralized can be established only by analysis for gold.

Gold in the unoxidized ore is invisible by reflected and transmitted light microscope at even high (up to 500×) magnifications and thus, can be referred to as "invisible" or "submicroscopic Au". Although gold is spatially closely associated with realgar, realgar separates contain little gold (<0.3 ppm). Chemical and microprobe analyses have shown that the invisible gold in the unoxidized ore may occur as: (1) coatings or thin films on arsenic-rich pyrite; (2) submicroscopic native gold inclusions in pyrite; and (3) submicroscopic particles in association with clay minerals and organic matter (Zheng, 1989; Zheng et al., 1993a; Gu, 1994a,c). In the oxidized to semioxidized ore from the upper 0–100 m of ore bodies, several grains of visible gold have been found (Gu, 1988). They generally occur as anhedral irregular particles along margins or within microfissures in pyrite, realgar, quartz or calcite, and range in size from less than 1 to 10 μm. They are chemically pure with a high gold-fineness of 894–964, which is comparable to those in the Ertaizi deposit (990, Liu and Geng, 1985), Banqi deposit (900, Liu and Geng, 1985), and Getang deposit (985, Liu et al., 1989) of sedimentary rock-hosted disseminated type in China, as well as the Carlin-type gold deposits in the western United States (>950, Yang, 1984) but distinguishable from the other epithermal type and subvolcanogene hydrothermal type gold deposits (680–760, Liu and Geng, 1985).

3.2. Qiaoqiaoshang gold deposit

The deposit is located in Songpan County, approximately 20 km southeastward from the Dongbeizhai deposit (Fig. 1), at an elevation between 3300 and 3600 m above sea level. This newly discovered deposit is presently being explored and drilled at different levels to evaluate its potential for production. Open-air ore leaching experiments are being carried out to provide a scientific basis for selecting an economical and effective treatment and extraction process for the ore.

The Xueshan E–W-trending fault zone passes through the mine district and separates the Middle–Upper Triassic turbiditic sandstone–siltstone–slate of the lower plate from the Upper Paleozoic carbonate rocks of the upper plate (Fig. 4). The main fault plane strikes roughly E–W, dips 65–80°N at shallow depths and about 45°N deeper. Movement on the branching faults made the lower plate sedimentary rocks folded and highly contorted; these faults were in turn crosscut by two sets of small-scale NE–SW- and NW–SE-trending normal faults or strike–slip faults.

Gold mineralization is confined to the lower plate of the Xueshan fault within the third (T^3_{2-3}) and sixth (T^6_{2-3}) units of the Middle–Upper Triassic. Petrographically, the host rock is remarkably similar to that of the Dongbeizhai deposit and characterized by a succession of slightly metamorphosed calcareous, dolomitic slate rhythmically interbedded with minor amounts of carbonaceous, argillaceous siltstone, and sandstone. It commonly contains enough diagenetic pyrite to be visible in hand specimens and high contents of carbonaceous materials to give the rock a black to dark gray color.

The deposit contains two ore zones and nine known ore bodies (Fig. 4). Ore bodies I and II are confined to the north ore zone, while the rest of the ore bodies occur in the south ore zone. The ore bodies are typically layer- or lens-like in shape with the attitudes similar to the host sedimentary rocks. They are 36–258 m long and 0.4–5.4 m thick and generally contain 2–3 g of gold per metric ton, with a maximum grade of 6.15 g per metric ton.

Similar to the Dongbeizhai deposit, pyrite and realgar are the most common sulfides in the Qiaoqiaoshang ore, although trace amounts of arsenopyrite, marcasite, stibnite, chalcopyrite, tetrahedrite, sphalerite, galena, scheelite, and bournonite are also present. On the basis of whether pyrite or realgar dominates the sulfide components, the primary

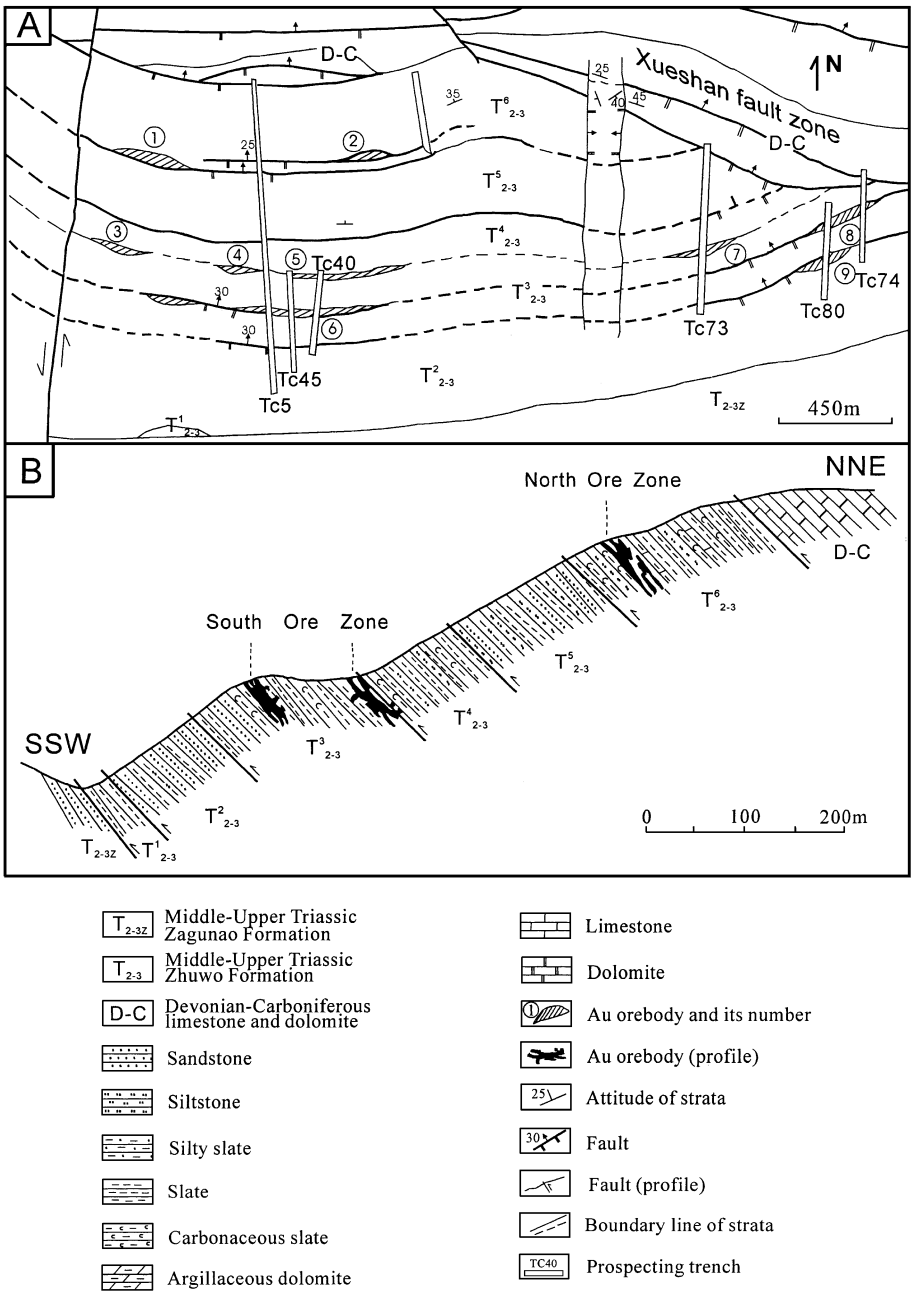

Fig. 4. (A) Generalized geologic map of the Qiaoqiaoshang gold deposit (after unpublished data of the 606 Geologic Team of the Southwestern Exploration Company of Metallurgical Geology, 1990). (B) A profile through the Qiaoqiaoshang gold deposit showing the south and north ore zones (after unpublished data of the 606 Geologic Team of the Southwestern Exploration Company of Metallurgical Geology, 1990).

unoxidized ore can be subdivided into pyrite– and realgar–gold ores. The former occurs in the south ore zone and local parts of the north ore zone, whereas the latter is only confined to ore bodies I and II of the north ore zone. No visible gold has been observed in either ore type.

3.3. Manaoke gold deposit

The Manaoke gold deposit is located in Nanping County (Fig. 1), at an elevation between 2700 and 3700 m. It was discovered as a result of a geochemical exploration and Au-anomaly detection program in 1990 and is now being evaluated for its economic potential.

Gold mineralization at Manaoke occurs within a 300-m-thick section of calcareous and silty slate of the middle unit of the Middle Triassic Zagashan Formation (T^2_{2zg}; Fig. 5). The immediate host rock is physi-

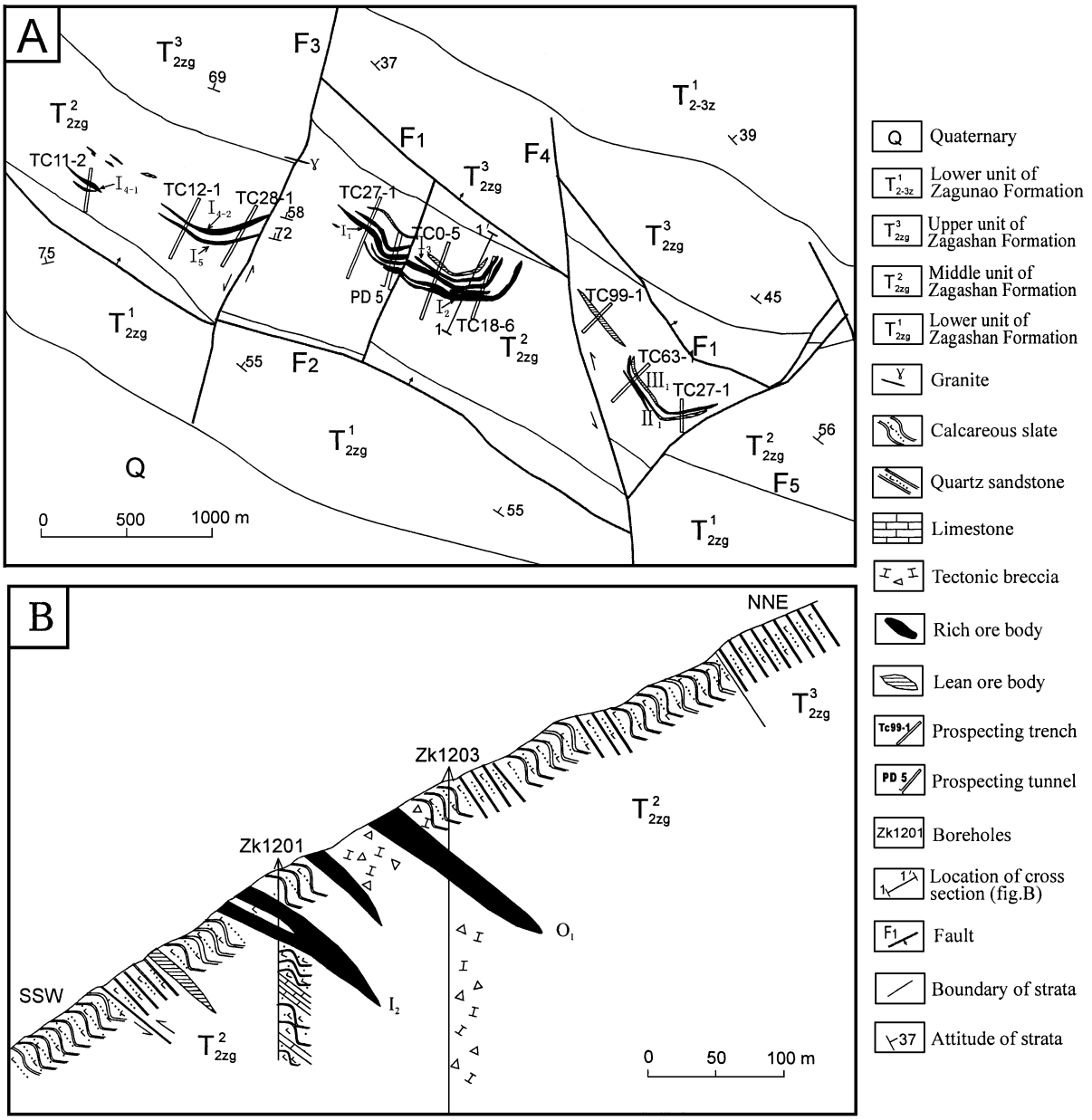

Fig. 5. Simplified geologic map (A) and cross-section (B) of the Manaoke gold deposit (after the 205 Geologic Team of NW Sichuan, 1990).

cally and mineralogically very similar to that of the Dongbeizhai and Qiaoqiaoshang deposits. Current prospecting has defined more than 10 stratiform ore bodies. The ore bodies are typically layer- or lens-like with attitudes similar to their host sedimentary rocks and commonly vary from 90 to 250 m in length and 1–6 m in thickness with gold grades of 4–10 g per metric ton. The largest ore body discovered to date is 365 m long, 2.4 m thick and extends 235 m along dip with an average grade of 5.89 g of gold per metric ton.

Stibnite, realgar, and scheelite are the most common ore minerals at Manaoke. Pyrite, arsenopyrite, and native gold are locally observed. Native gold was found only in the oxidized ores from the upper part of the ore bodies. It commonly occurs as flaky, filamentous or granular particles associated with limonite, siderite, and quartz and ranges in size from 1 to 50 μm with a maximum grain size of 180 μm. In the unoxidized ore, gold is intimately associated spatially with stibnite, realgar, and scheelite. Gangue minerals consist of quartz, calcite, dolomite, and ankerite. Limonite (mainly goethite), stibiconite, and valentinite are common in oxidized ores.

4. Ore fabrics

Although there exist some small differences in geological, petrological, mineralogical, and geochemical features among the described sedimentary rock-hosted disseminated gold deposits in NW Sichuan, ore fabrics of these deposits show considerable similarities. Macroscopically, all the deposits are confined to a definite horizon of several meters to less than 200 m in thickness of the Middle–Upper Triassic turbiditic sequence. The ore bodies are typically layer- or lens-like and parallel or subparallel to the stratification of the host sedimentary rocks with the length of tens to several hundreds of meters in strike (Fig. 6A,B). They grade both vertically and laterally to normal unmineralized sandstone, siltstone, and slate and show similarities in composition to the host rocks, except for their relatively higher contents of ore minerals such as pyrite, arsenopyrite, realgar, stibnite, and scheelite. Within a single stratabound ore layer essentially two ore types are recognized. One is the stratiform ore composed of rhythmical interbeds of sulfides such as pyrite, arsenopyrite, realgar, and stibnite and detrital quartz, quartzite, sericite, and graphite (Fig. 6D). It is commonly folded, deformed, and sheared concordantly with its country rocks (Fig. 6C). The other is the network ore characterized by numerous gold-bearing veins and veinlets of quartz–calcite–sulfide randomly filling fissures, microfissures, and cleavages parallel to or transecting bedding but still stratabound. Obviously, they must have been formed by different geologic processes.

Bearing these field geologic features in mind, microscopic ore fabrics have been investigated in detail. Since pyrite, realgar, and stibnite are the most abundant ore minerals in the studied deposits and intimately associated spatially with gold mineralization, our ore fabric study has been focused on these minerals.

4.1. Pyrite

Pyrite, in a variety of habits, is an ubiquitous sulfide in the deposits and makes up 0.3–6% of the ore. Detailed microscopic observations identified at least three generations of pyrite (Py-I to -III). Py-I is framboidal pyrite, a spheroidal aggregate of discrete, equigranular pyrite microcrysts (Fig. 7A). Numerous spheroids with diameters of 5–50 μm tend to be concentrated in narrow bands parallel to the bedding of host rocks and ores. The size of the microcrysts ranges from 0.1 to 3 μm and does not vary noticeably with that of the spheroids: the larger contains more microcrysts, the smaller fewer. The microcrysts may occur in the forms of octahedra, pentagonal dodecahedra, or cubes, and form ordered to non-ordered arrays. Framboidal pyrite spheroids were locally recrystallized or sammelkristallized (accretive crystallization) to idiomorphic crystals.

Py-II commonly occurs as relatively larger (from 5 μm up to 1–2 mm) euhedral to subhedral grains that are concentrated together with arsenopyrite and trace amounts of marcasite, chalcopyrite, tetrahedrite, and sphalerite in fine laminae parallel to the bedding (Fig. 7B–G). Pyrite laminae were locally sammelkristallized or recrystallized and concordantly folded or deformed with host rocks and/or ores, suggesting that such a recrystallization may have taken place during diagenetic process, namely predeformational recrys-

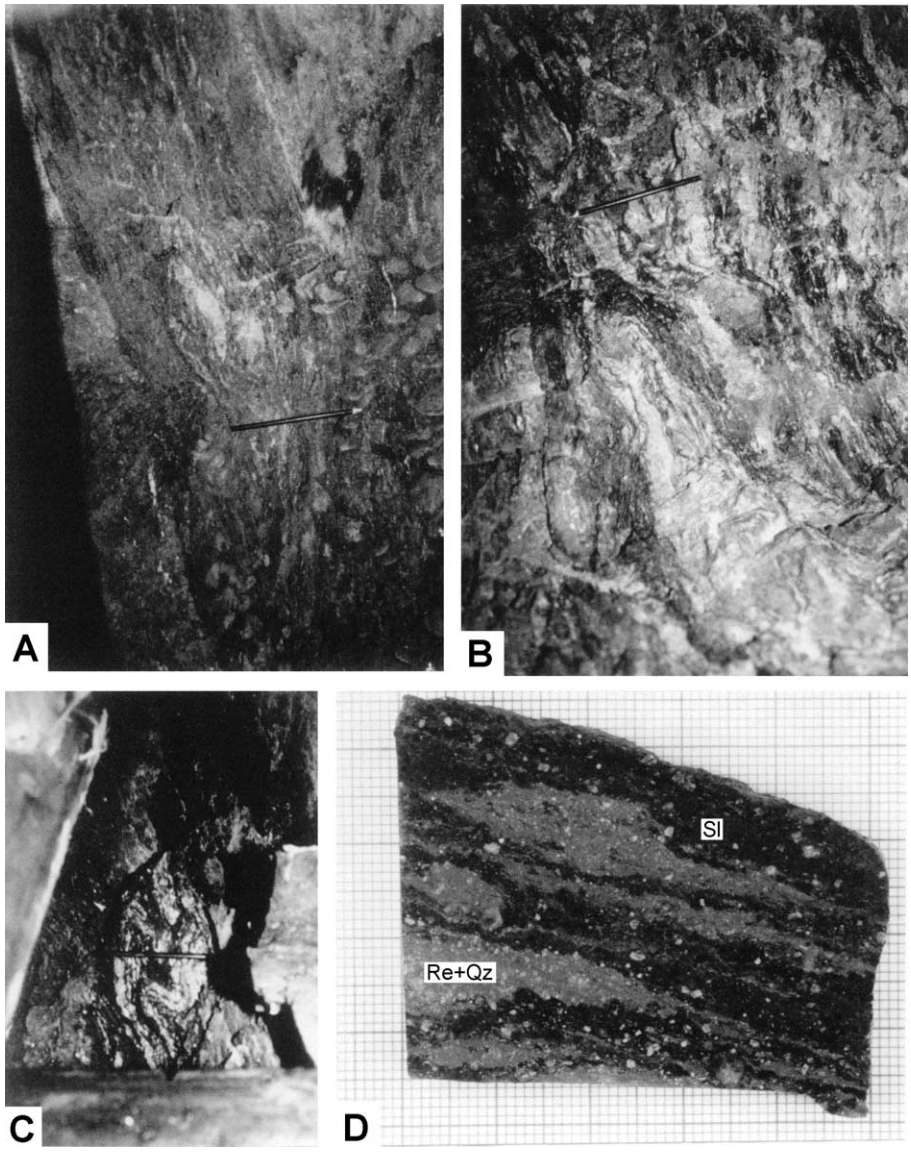

Fig. 6. Pit exposures and polished ore specimen showing typical characteristics of ores and host rocks in the Dongbeizhai (A–C) and Qiaoqiaoshang (D) deposits. (A) Fine-laminated realgar ore (light color) in carbonaceous sericitic slate. The ore fine lamination lies parallel to the stratification of the host rock (roughly vertical). The pencil for scale is 16 cm long. Pit exposure of a prospecting gallery at the level of 3424 m. (B) Enlargement of part of photograph A showing bedding-parallel realgar–quartz (light color) laminae interlayered with carbonaceous sericitic slates (dark color). (C) Fine-laminated realgar ore (light color) locally deformed and folded coincidently with the host carbonaceous sericitic slate. The pencil for scale is 16 cm long. Pit exposure of a prospecting gallery at the level of 3424 m. (D) Ore specimen from a stratiform ore body in the Qiaoqiaoshang deposit showing lens-like fine laminae of realgar (Re) and quartz (Qz) in carbonaceous sericitic slate (Sl, black to dark gray), millimeter paper for scale.

tallization. Sometimes ‘‘graded bedding’’, displayed by an upward decline of pyrite grain size within a single lamina, is well shown (Fig. 7C,E). This is a typical example of geopetal ore fabrics and suggests a synsedimentary origin (Sander, 1970). Another excellent phenomenon with significant genetic meaning is

that some sammelkristallized idioblasts of Py-II with pure recrystallization rims contain numerous microinclusions up to tens of microns across of quartz, quartzite, sericite, graphite, and rutile and display *s*-internal fabrics (cf., Sander, 1970; Fig. 7H). The orientation of these internal microinclusions is roughly parallel to the external stratification of the whole rocks and/or ores. This observation, together with the close spatial association of these pyrites with Py-I, as well as the "graded bedding" described above, strongly suggests a primary syngenetic origin of Py-II and its post-deformational (possibly diagenetic) recrystallization and/or accretive crystallization history.

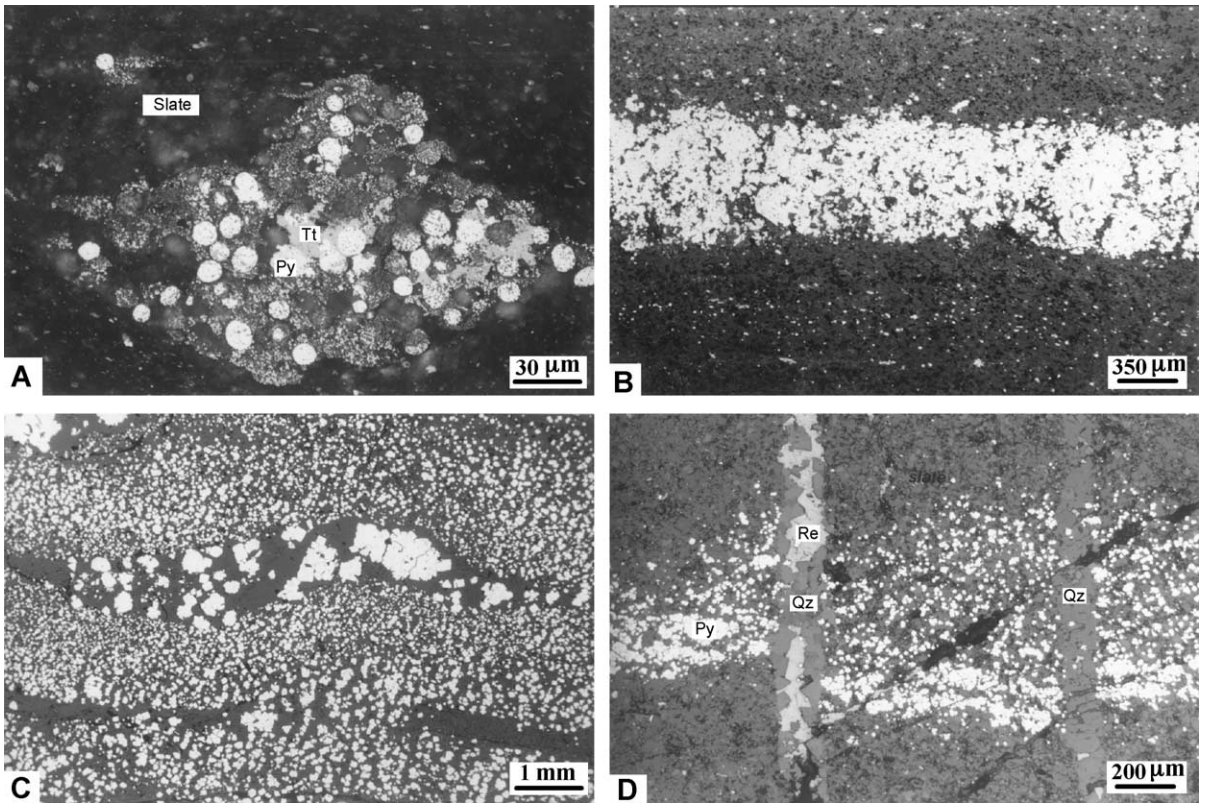

Fig. 7. Photomicrographs of pyrite fabrics. (A) A framboidal pyrite lens parallel to the stratification (horizontal) of slate (dark gray to black) and composed of pyrite spheroids (Py) associated with tetrahedrite (Tt). Note the local accretive crystallization (sammelkristallization) of framboidal spheroids. Qiaoqiaoshang deposit, polished section, oil immersion, 1 nicol. (B) Sulfides (light color) including pyrite, arsenopyrite, marcasite, chalcopyrite, and tetrahedrite concentrated in a fine lamina parallel to the stratification (horizontal) of slate (gray to dark gray). Tuanjie deposit, polished section, 1 nicol. (C) Fine-laminated pyrite showing local folding and predeformational accretive crystallization and/or recrystallization. Note the change of grain size of pyrite in a single lamina. Nanggai deposit, polished section, 1 nicol. (D) A pyrite (Py) lamina parallel to the stratification (horizontal) of slate and crosscut and dislocated by later formed quartz (Qz)–realgar (Re) veinlets. Dongbeizhai deposit, polished section, 1 nicol. (E) "Graded bedding" shown roughly by an upward decline of grain size of pyrite. The stratification of slate lies horizontally. Qiaoqiaoshang deposit, polished section, 1 nicol. (F) Fine crystalline pyrite (Py) concentrated in sericite (dark gray) fine laminae outlines the relict primary stratification (horizontal) of quartzitic slate (gray). *s*-discordant microfissures in the upper part of the photograph are filled by younger realgar (Re). Dongbeizhai deposit, polished section, 1 nicol. (G) In spite of accretive crystallization, rhythmical interbeds of realgar (Re), pyrite (Py), quartz (Qz), calcite (Cal), sericite (dark gray) and graphite (black) outline the relict stratification (horizontal) of ore. Dongbeizhai deposit, polished section, 1 nicol. (H) Sammelkristallized pyrite (Py) idioblasts with pure recrystallization rims contain microinclusions of quartz, sericite, and graphite and display *s*-internal fabric, which is roughly parallel to the stratification of the external host rock (quartzitic slate). Apy = arsenopyrite. Dongbeizhai deposit, polished section, 1 nicol.

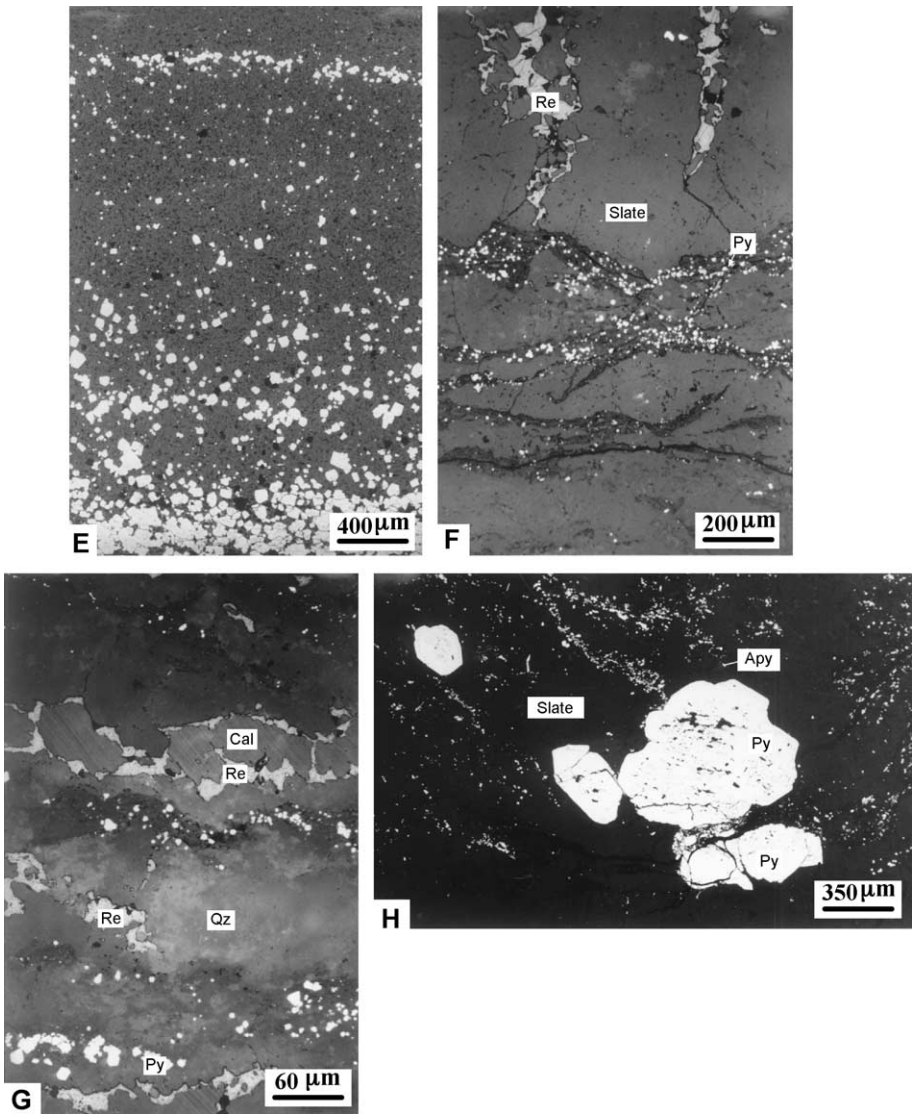

Fig. 7 (*continued*).

Both Py-I and -II were dislocated and crosscut by later formed quartz–calcite–sulfide veins and veinlets (Fig. 7D).

Py-III is present in veins and veinlets and usually intergrown with arsenopyrite, marcasite, quartz, and calcite. The veins range from less than 0.1 up to more than 5 mm in width. Pyrite grains of this type have both cubic and pyritohedral habits and usually show arsenic-rich overgrowth fabrics. It seems to be without question that Py-III was formed as a result of hydrothermal processes.

4.2. Realgar

In stratiform ores, orange to orange-yellow realgar occurs macroscopically as fine laminae or oriented lenses or "augen" interbedded with quartz, quartzite, sericite, and graphite, which were locally folded and

deformed coincidently with host rocks (Fig. 6). Under the microscope, two distribution patterns of realgar are recognized. Realgar commonly occurs as fine laminae consisting of micrograined crystallites rhythmically interbedded with allogenic components of quartz, quartzite, sericite, graphite, and heavy minerals such as tourmaline, rutile, titanite, and zircon (Fig. 8A–E). Realgar of this form is strictly concentrated in the fine laminae as intergranular cement or matrix. The fine lamination of ductile realgar locally bends around rigid detritus such as quartz and quartzite (Fig. 8A,B), and locally fine laminae of realgar are folded or deformed concordantly with detrital components (Fig. 8C). It is of great interest that such layer inhomogeneity (cf., Sander, 1970) is sometimes beautifully shown by the change of grain size of realgar

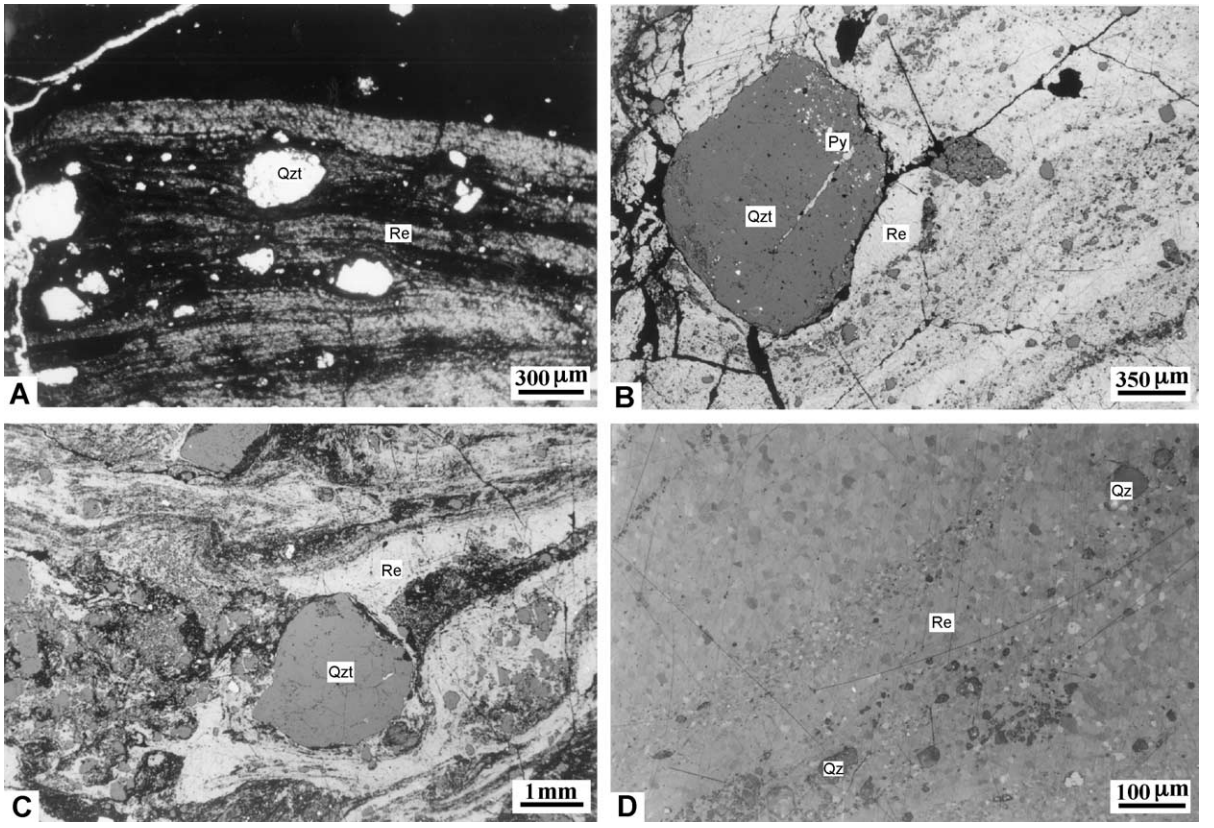

Fig. 8. Photomicrographs of realgar fabrics. (A) Fine-laminated realgar (Re) containing detrital components of quartz and quartzite (Qzt). Note the bending of realgar laminations around the rigid detritus of quartz and quartzite. Dongbeizhai deposit, thin section, 1 nicol. (B) Deformed relict fine laminations shown by the rhythmical interbeds of realgar (Re) and detrital components of quartz, pyrite (Py)-bearing quartzite (Qzt) and sericite (dark gray to black). Note also the bending of fine laminations around the rigid obstacles. Dongbeizhai deposit, polished section, 1 nicol. (C) Sericite–quartzite–realgar ore composed of detrital components of partly cataclastic quartzite, sericitic quartzite (Qzt), fine-laminated sericite (fine flaky) with graphite, and realgar (Re). As a fabric relict of primary sedimentary process, the mechanically anisotropic laminae exhibit monoclinic-symmetrical *s*-preferential flexure-slip folding and encircle rigid obstacles. Dongbeizhai deposit, polished section, 1 nicol. (D) Fine laminations (left bottom to right top) shown by the change of grain size of realgar (Re) and parallel alignment of detrital quartz (Qz). Qiaoqiaoshang deposit, polished section, nicols ×. (E) Layer inhomogeneity shown by the *s*-parallel alignment of detrital quartz, pyritiferous (white) quartzite (Qzt), sericite and graphite (fine flaky, dark gray and black) in realgar (Re). Dongbeizhai deposit, polished section, 1 nicol. (F) Fine crystalline realgar (Re) as pigments inhomogeneously disseminated in internal microfissures and intergranular rims of quartz (Qz). Manaoke deposit, polished section, oil immersion, nicols +. (G) Realgar (Re) pigments inhomogeneously aligned in subparallel lines within quartz (Qz). Manaoke deposit, polished section, oil immersion, nicols +. (H) Brecciated marcasite idioblast (Ma), quartz (Qz), calcite (Cal) and pyritifeous quartzite (Qzt) cemented by realgar (Re). Dongbeizhai deposit, polished section, nicols ×.

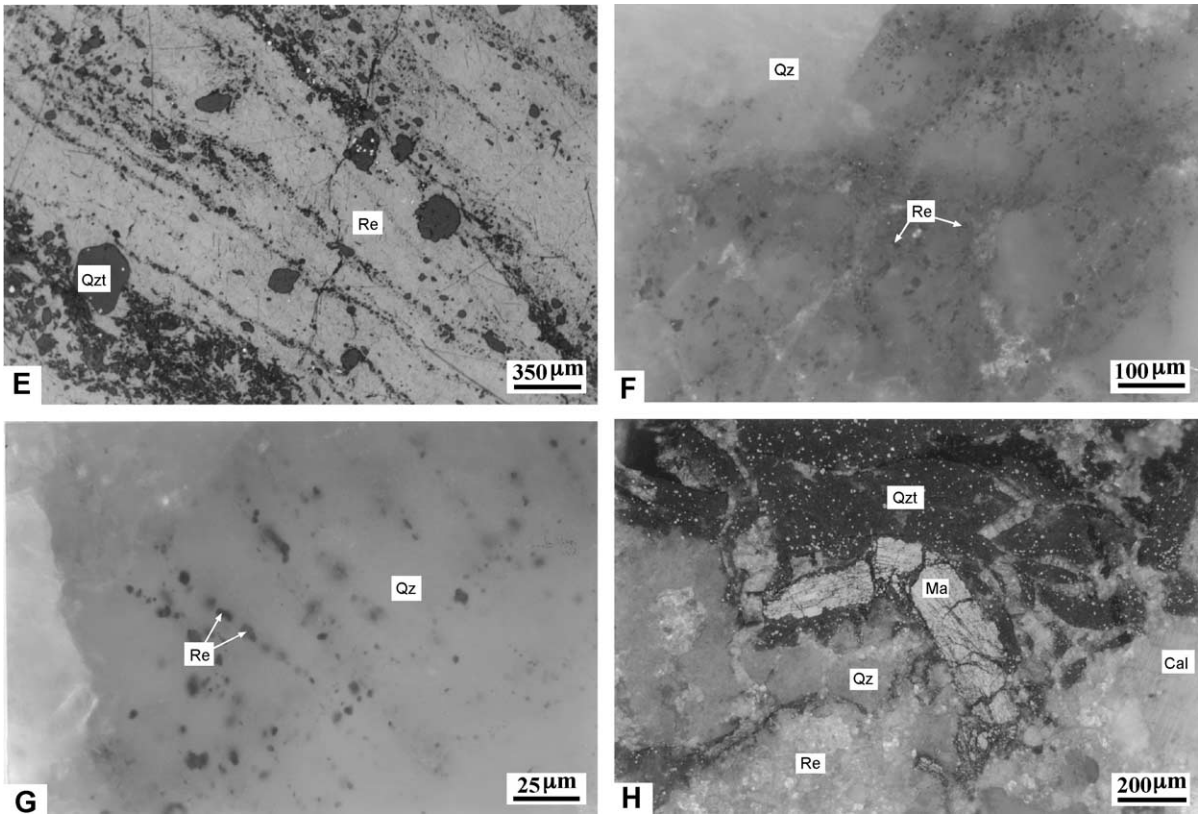

Fig. 8 (*continued*).

within a single lamina (Fig. 8D). That is, the micrograined (0.003–0.007 mm) sublaminae are interbedded with fine-grained (0.008–0.02 mm) and coarse-grained (0.03–0.1 mm) sublaminae in the sequence. It is also noteworthy that syn- to post-crystalline deformation and shearing overprints resulted in the statistical alignment of detrital components (Fig. 8E) and grain elongation (Kornlängung) of realgar crystallites (Zheng et al., 1993a; Gu, 1994a). The schistosity plane lies parallel both to the macrostratification and to the microlamination of the host rocks and/or ores.

The other distribution pattern of realgar in stratiform ores is that realgar occurs as extremely fine-grained (<0.01 mm) xenomorphic crystallites inhomogeneously disseminated within ‘‘red quartz’’, which in itself occurs as fine-laminated or oriented lenses or ‘‘augen’’ parallel or subparallel to the stratification of the ores/rocks and shows typical orange-yellow to yellow internal reflection according to the depth of the realgar pigments (Fig. 8F,G). Detailed microscopic examinations indicate that such realgar pigments either occur in internal microfissures and intergranular rims of quartz (Fig. 8F) or are inhomogeneously aligned in subparallel lines within quartz (Fig. 8G). The former seems to be post-deformational crystallites, while the latter may have coprecipitated with quartz. However, a complete understanding of the genesis of these realgar pigments still waits for further investigation.

Realgar in the network ore commonly occurs in veins and veinlets ranging in size from a few millimeters wide following microfissures (Fig. 7D,F), to as wide as 20 cm in open fractures and joints. Realgar of this generation also occurs as cement for mineralized deformation breccia (Fig. 8H). Compared to the fine-laminated realgar, the syn- to post-deformational crystallites of realgar described here have much coarser grain size (0.1–1 mm).

4.3. Stibnite

Stibnite is the most abundant ore mineral in the Manaoke gold deposit, although in other deposits such as Dongbeizhai and Qiaoqiaoshang it is less important. On the one hand, stibnite occurs as fine laminae rhythmically interbedded with realgar, pyrite, arsenopyrite, and scheelite as well as quartz, calcite, sericite, and graphite (Fig. 9A–C). On the other hand, it also occurs as stratabound networks with veins and veinlets randomly filling fissures, microfissures, and cleavages of the shattered host rocks, or as cement of mineralized deformational breccia (Fig. 9D).

Relict fabrics of sedimentary origin are observed in the macroscopically massive or banded stibnite–quartz ores (Gu, 2000). Under the microscope, quartz occurs as separate but oriented in subparallel lines, idiomorphic to hypidiomorphic, equidimensional grains of 0.05–0.25 mm in diameter (Fig. 9A), and locally as small aggregates or disseminated grains. The cross-section of these quartz components usually has a short prismatic habit and shows authigenic features. The fine lamination shown by the layer inhomogeneity of quartz is in agreement with the stratification of the ores and host rocks and represents a relict fabric of sedimentary origin.

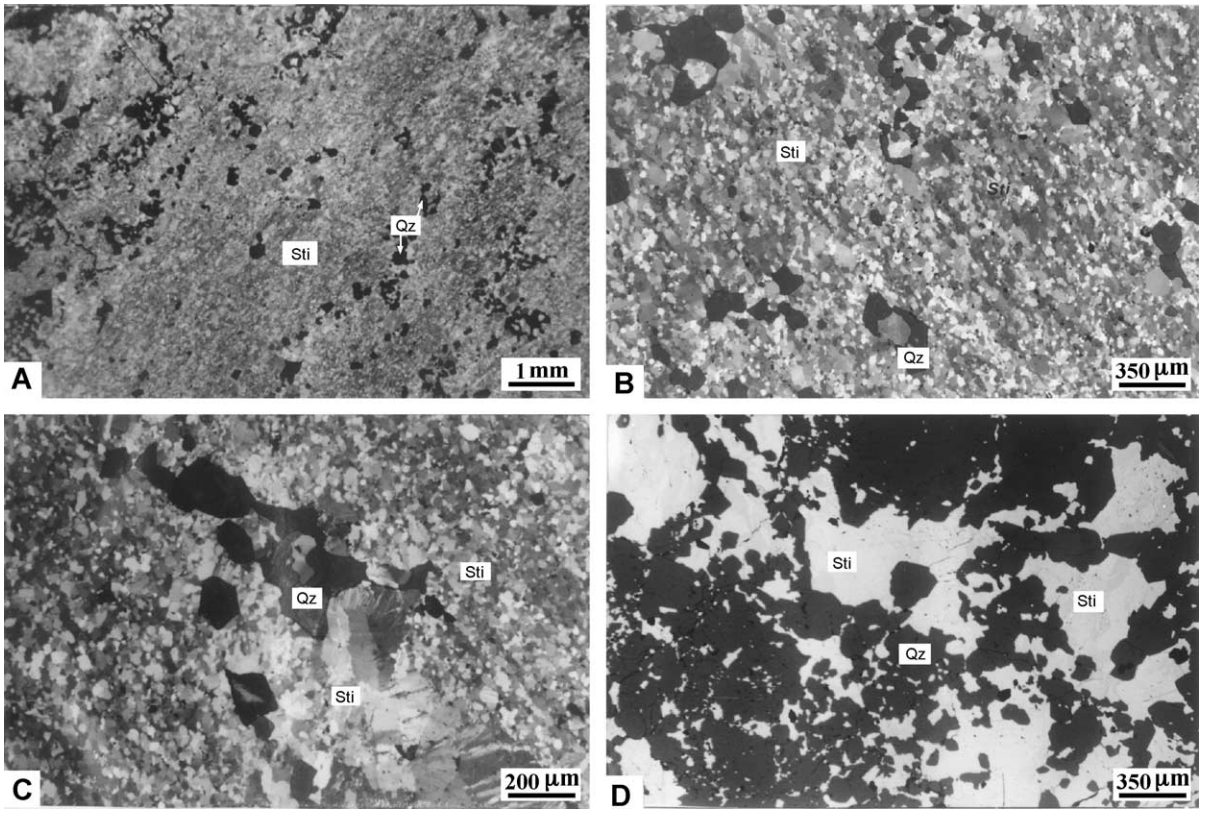

Fig. 9. Photomicrographs of stibnite fabrics in the ore of the Manaoke deposit. (A) Fine-laminated structure shown by the interbeds of stibnite crystallites (Sti) and idiomorphic to hypidiomorphic quartz crystals (Qz). The schistosity plane *s* (left bottom to right top) shown by the grain elongation and statistical alignment of stibnite grains lies parallel to the relict sedimentary quartz lamination. Polished section, nicols ×. (B) Grain elongation and orientation of stibnite crystallites (Sti) caused by intragranular deformation. The dark gray to black grains are idiomorphic to hypidiomorphic authigenic quartz (Qz). Polished section, nicols ×. (C) Intragranular deformation of stibnite (Sti) results in grain elongation and orientation along schistosity planes (left top to right bottom). Discrete change of stibnite grain size (right-angled to the *s* plane) suggests the existence of a predecessor fabric of stibnite, most probably a primary synsedimentary stage. Qz = quartz. Polished section, nicols ×. (D) Cataclastic quartz (Qz) cemented and replaced by stibnite (Stib). Polished section, 1 nicol.

The layer inhomogeneity of the closed stibnite crystallites is of more significant meaning. Fine-grained stibnite crystals vary from 0.005 to 0.2 mm in grain size and statistically display grain elongation in the two-dimensional section (Fig. 9B). This intragranular deformation in the lattice of the crystallites is shown by a distinct aggregate polarization statistically seen to have uniform extinction and brightness positions under the crossed polars of a microscope. In general, such a layer inhomogeneity extends roughly parallel to the fine lamination shown by the authigenic quartz crystals.

Locally, the layer inhomogeneity in the closed stibnite fabric is shown by the change of grain size of crystals (Fig. 9C), namely the micrograined (e.g., 0.005 mm) fine laminae of stibnite interbedding with fine-grained (e.g., 0.01–0.02 mm) and coarse-grained (e.g., 0.07–0.2 mm) stibnite laminae. The fine lamination shown by the change of grain size is parallel or subparallel to the preserved fine stratification shown by the authigenic quartz crystals.

It is noted that stibnite crystallites often show intense undulating extinction and local schistosity (Lamellierung) through translation. These are obviously due to the mechanical influence of tectonism, namely post-crystalline deformation, and constitute, together with the grain elongation and aggregate polarization, a typical feature of tectonic fabrics. But we have also noted that extremely fine-grained (only several microns in grain size) *s*-parallel oriented stibnite microlites without undulating extinction are developed in the stibnite ore in the schistosity zone and in the lattice dislocation zone of the stibnite aggregates. They are suspected of being post-deformational recrystallites. In other words, after diagenesis and weak metamorphism, there probably exists a selective mimetic crystallization of "stibnite by stibnite" without chemical changes of major mineral and major element compositions.

5. Discussion of ore genesis

Zheng (1989), Zheng et al. (1990, 1991, 1993b,c, 1994), Li et al. (1991) and Wang (1995) noted the similarities between sedimentary rock-hosted disseminated gold deposits in NW Sichuan and the Carlin-type gold deposits in the western United States and elsewhere. They proposed an epigenetic model for the gold deposits in NW Sichuan that is similar to the genetic model proposed by many investigators (e.g., Radtke et al., 1974, 1980; Radtke, 1985; Percival et al., 1988; Jewell and Parry, 1987; Arehart et al., 1993; Ilchik and Barton, 1997) and referred to these deposits as "underground hydrothermal (brine) leaching Carlin-type gold deposits". Synsedimentary processes have been believed to result in only a "diffuse pre-enrichment of metals in sediments", and "the industrial ore enrichment took place as a result of intensive thermal mobilization through circulating meteoric waters" during the Late Cretaceous (Zheng et al., 1994).

Our study of the ore fabrics of these deposits, however, suggests an alternative genetic model in which we believe that stratiform ores were formed simultaneously with their host Middle–Upper Triassic sedimentary rocks by nonvolcanic hydrothermal exhalation (submarine hot spring environments) on the seafloor, while vein–veinlet or network mineralization was formed as the result of remobilization or reworking of the pre-existing stratiform ores by complicated processes such as diagenesis, weak metamorphism, tectonic deformation, and epigenetic hydrothermal activity.

As mentioned above, a common characteristic of these deposits is that the ore bodies are layer- or lens-like in shape and generally parallel to the stratification of the host sedimentary rocks with the length of tens to several hundred meters in strike (Figs. 3–6). They are commonly confined to a definite horizon in the Triassic turbiditic sequence. Stratiform ore layers were folded, deformed, and sheared coincidently with country rocks and grade both vertically and laterally to the normal unmineralized rocks, except for their relatively higher contents of ore minerals such as pyrite, arsenopyrite, realgar, stibnite, and scheelite. Fine-laminated structures shown by rhythmical interbeds of sulfides and allogenic detrital quartz, quartzite, sericite, and graphite are well developed. These macroscopic features suggest the simultaneity of chemical precipitation of ore minerals and mechanical sedimentation of detrital components.

Since pyrite, realgar, and stibnite are the most abundant sulfides in the studied deposits and are spatially intimately associated with gold mineraliza-

tion, detailed studies of microfabrics of these minerals provide important information concerning the genesis of deposits.

Relatively immobile and hard minerals such as pyrite, arsenopyrite, and marcasite have been found to be useful tools for genetic interpretation because they represent the mediator to pre-existing primary fabrics (Zheng et al., 1993a; Gu, 1994a). Pyrite most commonly occurs either as framboidal spheroids (Py-I) or as fine laminae (Py-II) typically parallel to the bedding and locally showing "graded bedding" structure and *si* "internal sedimentary" (cf., Sander, 1970) fabric (Fig. 7), strongly suggesting syngenetic origin, although pyrites observed today have been subjected to accretive crystallization and recrystallization to a greater or smaller extent.

In contrast to pyrite, realgar and stibnite belong to mechanically and chemically extremely sensitive minerals and are thus commonly characterized by numerous veins and veinlets of millimeter-, centimeter-, decimeter-, and even meter-scales filling fissures, microfissures, and cleavages or occur as cement of mineralized breccia in the studied deposits. However, abundant relict fabrics of sedimentary origin are well-preserved in ores, especially in the fine-laminated stratiform ores. Such relict fabrics are readily shown either by rhythmical interbeds of both authigenic and allogenic components (Figs. 8A–C and 9A) or by the change of grain size of the same minerals (Figs. 8D and 9C). The layer inhomogeneity of fine-laminated realgar and stibnite is made more clear by occasionally parallel overprints of later schistosity planes. Thus, distinct grain orientation and elongation, aggregate polarization, and undulating extinction are well-developed (Figs. 8E and 9A–C).

Subsequent to sedimentation and diagenesis, weak metamorphism, tectonic deformation as well as epigenetic hydrothermal activity might have significantly remolded the stratiform ores and complicated primary synsedimentary ore fabrics. On the one hand, stratiform ore layers are folded, deformed or locally shattered, together with their host sediments. Brittle minerals such as pyrite, marcasite, and arsenopyrite commonly show cataclastic deformational fabrics, while the more ductile minerals, particularly realgar, stibnite, and calcite were subjected to intense folding, corrugation, and intragranular deformation. On the other hand, hydrothermal dissolution resulted in mobilization, transportation, and reprecipitation of ore-forming materials within stratiform ore layers, thus forming network mineralization in structurally controlled sites (fold hinges, shear zones, fissures, and cleavages, etc.) in the vicinity of the ore horizons.

The genetic model of the stratiform ores in the gold deposits are of syngenetic origin, while the network mineralization was formed as a result of remobilization of the pre-existing primary stratiform ores also gains support from geochemical data (Gu, 1994a, 1996). Ores and host rocks are similar in major and trace element compositions, except for the relatively

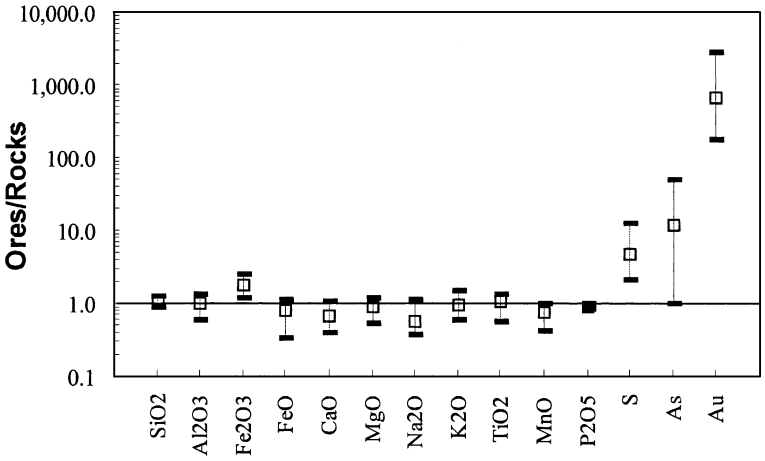

Fig. 10. Comparison of major and some trace elements between ores (sample number, $n = 18$) and host rocks ($n = 9$). Vertical lines show ranges and average values (squares) of the ore.

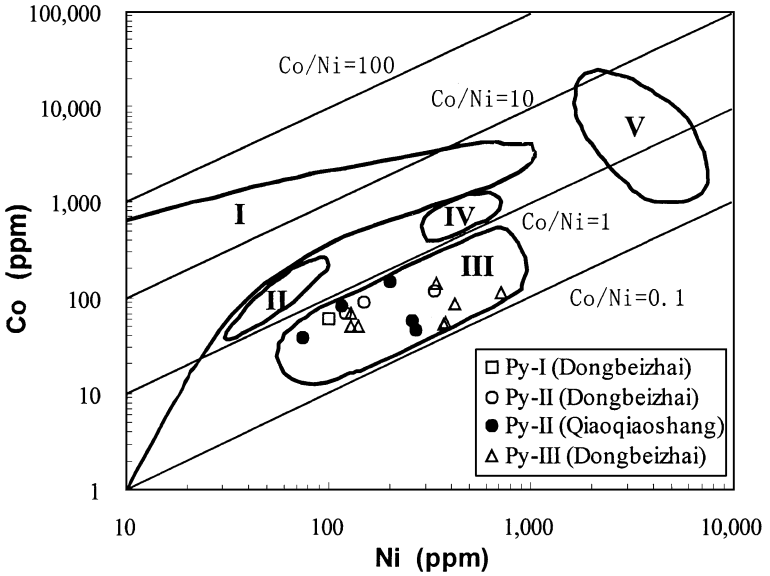

Fig. 11. Plot of Co versus Ni for genetic discrimination of pyrite. Data for the pyrite of various geneses after Bralia et al. (1979) and Bajwah et al. (1987). I—Submarine exhalative deposits; II—hydrothermal pyrites mobilized from massive sulfide ores; III—sedimentary environments; IV—Skarn deposits; V—magmatic deposits.

higher contents of ore-forming elements (Au, Ag, As, Sb, W, S, and Fe) in the ore (Fig. 10), suggesting the intimate relationship in genesis between ores and host rocks. Pyrite displays low Co/Ni ratios (0.14–0.60 at Dongbeizhai and 0.17–0.75 at Qiaoqiaoshang) and low contents of Co (<140 ppm, commonly <100 ppm) and Ni (commonly 100–400 ppm; Fig. 11), similar to those of sedimentary pyrite (Bralia et al., 1979) but distinguished from those of pyrites from submarine volcanic-exhalative massive sulfide deposits (Price, 1972; Bralia et al., 1979) and those of magmatic pyrite (Bajwah et al., 1987). Electron microprobe analyses (EMPA) have shown that different pyrite generations have no distinct differences in the concentrations of Fe, S, and As, except for relatively lower As contents in Py-I without detectable

Table 2
Mineral chemistry and concentrations of Au and As in minerals of the Dongbeizhai deposit analyzed by EMPA

Mineral	Analyzed spots	Spots with detectable Au									Spots without detectable Au						
		Spots	Au (%)		As (%)		S (%)		Fe (%)		Spots	As (%)		S (%)		Fe (%)	
			Average	± SD	Average	± SD	Average	± SD	Average	± SD		Average	± SD	Average	± SD	Average	± SD
Py-I	20	4	0.34	0.22	3.98	4.30	50.57	1.96	43.70	0.86	16	0.78	1.63	53.15	1.35	44.79	0.90
Py-II	65	13	0.33	0.25	4.49	3.96	50.50	2.49	43.77	1.31	52	4.39	4.01	50.47	2.78	43.76	1.56
Py-III	112	43	0.27	0.10	4.83	3.80	50.04	2.73	42.64	1.50	69	3.83	3.90	50.99	2.85	43.60	1.80
Re	14	3	0.15	0.12	66.58	2.08	31.19	1.86	0.06	0.08	11	65.84	2.18	31.12	0.98	0.03	0.05
Apy	45	10	0.42	0.22	42.70	1.81	22.19	0.62	32.33	0.92	35	41.90	3.22	23.55	3.10	32.90	1.32
Ma	11	6	0.44	0.30	0.41	0.76	53.09	1.75	44.20	1.69	5	0.37	0.43	52.91	0.88	44.50	0.50

The analyses were performed on an ARL-SEMQ electron microprobe equipped with a NORAN-VOYAGER energy-dispersive spectrometer (EDS) system at the Institute of Mineralogy and Petrography, University of Innsbruck, Austria. The instrument was operated at 15 kV (accelerating voltage) with beam current 20 nA, using the following X-ray lines and standards: Fe–Kα (metal), S–Kα (troilite), As–Lα (arsenic), Au–Mα (metal). The counting time was set at 200 s.

Abbreviations: SD = standard deviation, Py = pyrite (I, II, and III represent different generations), Re = realgar, Apy = arsenopyrite, Ma = marcasite.

Au (Table 2). Although hydrothermal pyrites (Py-III) seem to statistically have more detectable Au than those of sedimentary origin (Py-I and -II), Au contents are considerably variable from point to point even within a single grain, and are on the average comparable among different generations. This suggests that the gold most probably occurs as submicron inclusions in pyrites. No correlations between Au versus As and Fe versus S were observed (Fig. 12), as reported in other sedimentary rock-host disseminated gold deposits (e.g., Wells and Mullens, 1973; Mao, 1991; Fleet et al., 1993). The marked negative correlation between As and S ($r=-0.96$; Fig. 12) is indicative of substitution of S by As in pyrites.

Sulfur isotope data of pyrite, realgar, and stibnite from Dongbeizhai indicate that the ultimate source of sulfur in sulfides is seawater sulfates. The δ^{34}S values of sedimentary pyrites (Py-I and -II) range from -1.9‰ to 3.1‰ with an average of 1.8‰ (Fig. 13), consistent with the δ^{34}S value of a non-ore sedimentary pyrite at Qiaoqiaoshang (-0.2‰) reported by Hu (1991). We interpret these data to represent a major contribution of marine sulfur, because the δ^{34}S value of sulfur caused by bacterial reduction of marine sulfates is usually 15–25‰ (Sangster, 1976; Ohmoto and Rye, 1979) lower than that of seawater sulfates (about 20‰ during Mesozoic; Holser and Kaplan, 1966; Claypool et al., 1980). The δ^{34}S values of hydrothermal pyrites (Py-III) vary between -7.4‰ and 6.3‰, commonly between -4.4‰ and 2.9‰, with an average of -0.1‰, corresponding to the average value of sedimentary pyrite. Since it is difficult to isotopically rehomogenize sulfides (Bachinski, 1978), the local rehomogeni-

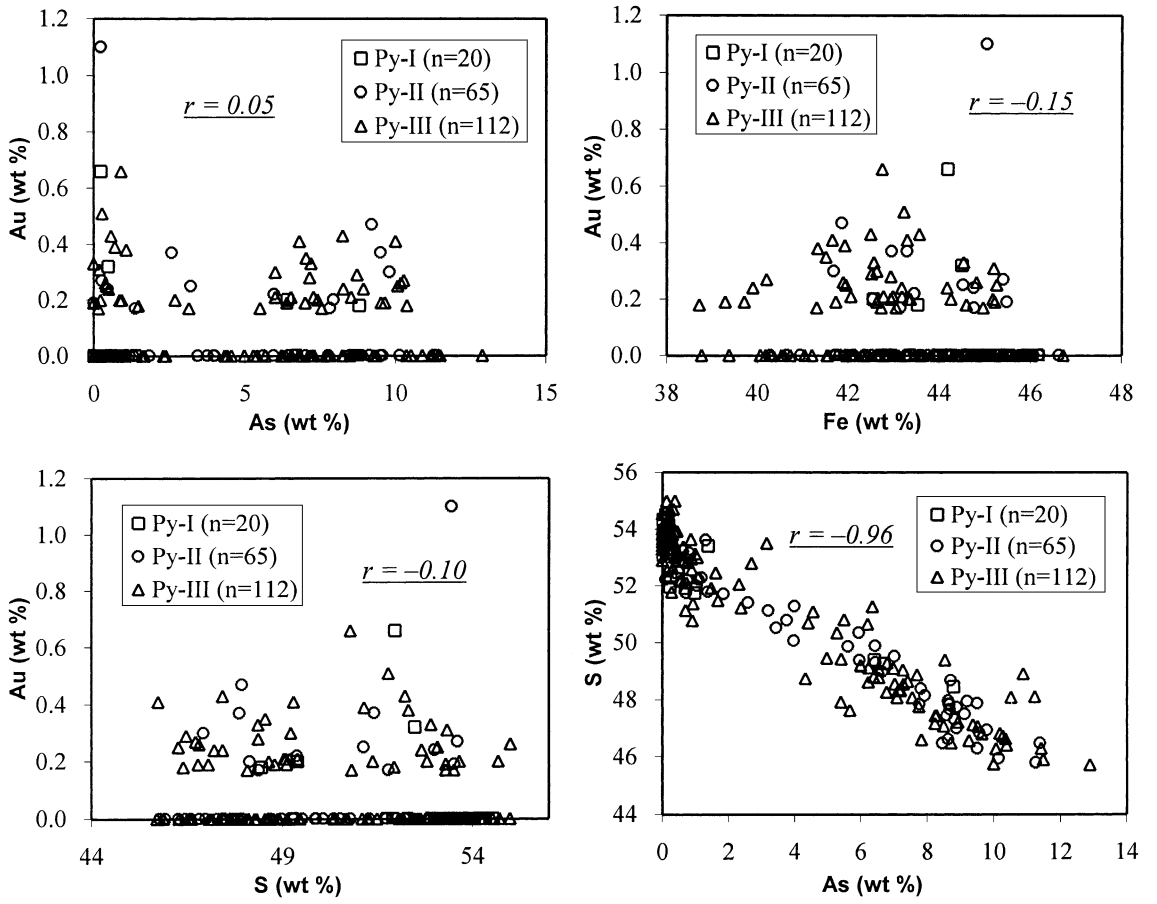

Fig. 12. Plots of As–Au, Fe–Au, S–Au, and As–S for the pyrite at Dongbeizhai analyzed by EMPA.

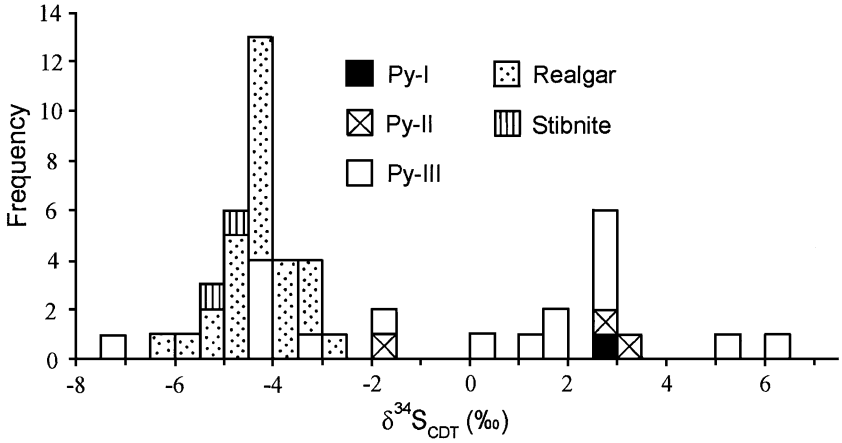

Fig. 13. Histogram of $\delta^{34}S_{CDT}$ values for sulfides in the Dongbeizhai gold deposit.

zation between sedimentary and hydrothermal pyrites could be eliminated from consideration. Therefore, the similarity in sulfur isotopic composition among different pyrite generations suggests that the hydrothermal pyrite (network ore) was formed as the result of the remobilization of sedimentary pyrite (stratiform ore). The $\delta^{34}S$ values of realgar and stibnite are approximately 5‰ lower than those of pyrite, probably due to the lower oxidation state of $[S]^{2-}$ in realgar and stibnite relative to the $[S_2]^{2-}$ in pyrite as well as the lower bond strength of As–S and Sb–S than Fe–S, because the heavy sulfur ^{34}S is preferentially enriched in the sulfides with higher oxidation state and higher bond strength (Bachinski, 1969).

Zheng et al. (1991) reported lead isotope model ages of a diagenetic pyrite (193 Ma) and three vein stibnite samples (192–218 Ma, average 203 Ma) from Dongbeizhai, which are in agreement with the Middle–Late Triassic age of the host sedimentary rocks. Recent work on Rb–Sr isotopes of fluid inclusions in quartz from the Manaoke stratiform ores by Fu (2000) has revealed that the initial $^{87}Sr/^{86}Sr$ ratio of the fluids (0.7085) is consistent with the $^{87}Sr/^{86}Sr$ ratio of seawaters (0.7090; Faure, 1986). Five samples outlined a Rb–Sr isochron age of 210 ± 11 Ma, consistent with the lead isotope model ages of sulfides at Dongbeizhai.

It is thus suggested that a submarine synsedimentary model, similar to that proposed by Emsbo et al. (1999) for the recently discovered gold occurrences on the Carlin trend, may more reasonably explain the macroscopic and microscopic as well as geologic and geochemical features of the sedimentary rock-hosted gold deposits in NW Sichuan. The significance of ore formation by exhalation on the seafloor is now almost universally accepted (e.g., Bonatti, 1975; Bonatti et al., 1976; Hekinian et al., 1980; Hutchinson, 1982; Cann and Strens, 1982; Rona, 1984; Cann et al., 1985; Hannington et al., 1986; Hannington and Scott, 1988, 1989; Rona et al., 1983; Huston and Large, 1989; Large et al., 1989; German, 1989; Leblanc and Billaud, 1990; Cook et al., 1990; Large, 1992; Cas, 1992). Volcanic-associated exhalation is considered to be commonly related to the formation of massive sulfide ores and typically accompanied by the presence of exhalites such as Fe–Si-rich chemical sediments, baritic rocks, tourmalite, and Fe–Mg oxides. Chlorite-enriched rocks are also a common feature in the exhalative systems (Leblanc and Billaud, 1990). In the studied deposits in NW Sichuan, however, typical exhalites are almost completely absent. Moreover, hardly any submarine volcanic rocks occur within the ore-bearing horizons. Therefore, the supply of the ore materials in the studied gold deposits during Triassic time seems to be most probably related to nonvolcanic submarine hydrothermal exhalative (something like "hot spring") processes.

Consequently, it is proposed that contemporaneous with the deposition of the sediments within the Bayanhar–Songpan–Ganze back arc basin, convecting thermal seawaters leached gold and associated elements such as Ag, As, Sb, W, Fe, and S from underlying rocks and precipitated them upon reaching

the seafloor in the vicinity of vents. Localization and concentration of ores may have been controlled by topography of the seafloor (Turner and Gustafson, 1978). The ore deposition was accompanied by rhythmical detrital sedimentation. At the scale of the whole studied district, there were likely several stages of exhalative activity, resulting in the deposition of several mineralized horizons during the evolution of the sedimentary basin. At the scale of a deposit or a single mineralized horizon, as shown in the deposits of Qiaoqiaoshang and Dongbeizhai, there is an evidence of a pulsative exhalative system showing a cyclic evolution of the metalliferous brines leading to successive deposition of pyrite ore and then of realgar–stibnite ore. From the viewpoint of sedimentology, the main mineralized horizons occur in the upper part of the submarine fan sequence where turbiditic sedimentation diminished, whereas hemipelagic to pelagic deposition predominated. For example, the Dongbeizhai and Qiaoqiaoshang ores occur in the upper parts of the Xinduqiao and Zhuwo formations, respectively. The host rocks are characterized by calcareous, sericitic slate interbedded with only small amounts of carbonaceous siltstone and sandstone. In contrast, mineralized horizons in other deposits such as Manaoke, Zheboshan, and Tuanjie occur in the stratigraphically lower level of the Middle–Upper Triassic turbidites where sandstone and siltstone constitute the major rock type. Consequently, these deposits are inferior to the Dongbeizhai and Qiaoqiaoshang deposits in both the intensity of mineralization and the ore reserve. The poor mineralization in sandstone- and siltstone-rich sediments may be attributed to the dilution of the sulfide components during the rapid turbiditic sedimentation.

Acknowledgements

Most of this work was carried out during the stay of the first author as a visiting scholar at the Institute of Mineralogy and Petrography, University of Innsbruck (Austria) from 1991 to 1994 and from 1997 to 1999. Sincere thanks are due to all the staff members of the institute, especially to the head Prof. Dr. P. Mirwald for his permission to use the facilities, Prof. Dr. F. Purtscheller for providing guidance of the work, and Mr. H. Rinner for preparing the thin- and polished-sections used in this study. We are grateful to Prof. B. Zhang and Prof. X.H. Xu for their numerous helpful and constructive discussions. The paper has benefited from critical reviews and insightful handling by G.B. Arehart, R.P. Ilchik, H. Foerster, and T. Horscroft. The research was supported by the National Science Foundation of China (NSFC) under the grants 49872038 and 49602029, the Scientific Research Foundation of Austria (FWF) under the grant P12026-GEO, the Ministry of Science and Technology of China under the grant G1999043210, and Chinese Academy of Sciences under a special grant for young national scientists. The first author was also supported by a grant from the Austrian Academic Exchange Service (ÖAD), which is greatly appreciated.

References

Arehart, G.B., 1996. Characteristics and origin of sediment-hosted disseminated gold deposits: a review. Ore Geol. Rev. 11, 383–403.

Arehart, G.B., Chryssoulis, S.L., Kesler, S.E., 1993. Gold and arsenic in iron sulfides from sedimentary rock-hosted disseminated gold deposits: implications for depositional processes. Econ. Geol. 88, 171–185.

Ashley, R.P., Cunningham, C.G., Bostick, N.H., Dean, W.E., Chou, I.-M., 1991. Geology and geochemistry of three sedimentary-rock-hosted disseminated gold deposits in Guizhou Province, People's Republic of China. Ore Geol. Rev. 6, 133–151.

Bachinski, D.J., 1969. Bond strength and sulfur isotopic fractionation in co-existing sulfides. Econ. Geol. 64, 56–65.

Bachinski, D.J., 1978. Sulfur isotopic composition of thermally metamorphosed cupriferous iron sulfide ores associated with cordierite–anthophyllite rocks, Gull Pond, Newfoundland. Econ. Geol. 73, 64–72.

Bagby, B.M., Berger, B.R., 1985. Geologic characteristics of sediment-hosted, disseminated precious metal deposits in the western United States. Rev. Econ. Geol. 2, 169–202.

Bajwah, Z.U., Seccombe, P.K., Offler, R., 1987. Trace element distribution, Co:Ni ratios and genesis of the Big Cadia iron–copper deposit, New South Wales, Australia. Miner. Depos. 22, 292–300.

Bonatti, E., 1975. Metallogenesis at oceanic spreading centers. Annu. Rev. Earth Planet. Sci. 3, 401–431.

Bonatti, E., Honnorez-Guerstein, M.G., Honnorez, J., Stern, C., 1976. Hydrothermal pyrite concretions from the Romanche trench (equatorial Atlantic): metallogenesis in oceanic fracture zones. Earth Planet. Sci. Lett. 32, 1–10.

Bralia, A., Sabatini, G., Troja, F., 1979. A revaluation of the Co/Ni ratio in pyrite as geochemical tool in ore genesis problems. Miner. Depos. 14, 353–374.

Cann, J.R., Strens, M.R., 1982. Black smokers and freezing magma. Nature 298, 147–149.

Cann, J.R., Strens, M.R., Rice, A., 1985. A simple magma-driven thermal balance model for the formation of volcanic massive sulphides. Earth Planet. Sci. Lett. 76, 123–134.

Cas, R.A.F., 1992. Submarine volcanism: eruption styles, products, and relevance to understanding the host-rock successions to volcanic-hosted massive deposit. Econ. Geol. 87, 511–541.

Claypool, G.E., Holser, W.T., Kaplan, I.R., Sakai, H., Zak, I., 1980. The age curves of sulfur and oxygen isotopes in marine sulfate and their mutual interpretation. Chem. Geol. 28, 199–260.

Cook, N.J., Halls, C., Kaspersen, P.O., 1990. The geology of the Sulitjelma ore field, northern Norway—some new interpretations. Econ. Geol. 85, 1720–1737.

Cunningham, C.G., Ashley, R.P., Chou, I.M., Huang, Z., Wan, C., Li, W., 1988. Newly discovered sedimentary rock-hosted disseminated gold deposits in the People's Republic of China. Econ. Geol. 83, 1462–1467.

Emsbo, P., Hutchinson, R.W., Hofstra, A.H., Volk, J.A., Bettles, K.H., Baschuk, G.J., Johnson, C.A., 1999. Syngenetic Au on the Carlin trend: implications for Carlin-type deposits. Geology 27, 59–62.

Faure, G., 1986. Principles of Isotope Geology, 2nd ed. Wiley, New York. 589 pp.

Feng, S., 1982. Characteristics of ore textures in a "Carlin type" gold deposit in Shaanxi. Geol. Prospect., 14–20 (in Chinese).

Fleet, M.E., Chryssoulis, S.L., MacLean, P.J., Davidson, R., Weisener, C.G., 1993. Arsenian pyrite from gold deposits: Au and As distribution investigated by SIMS and EMP, and color staining and surface oxidation by XPS and LIMS. Can. Mineral. 32, 1–17.

Fu, S.H., 2000. Study of gold-bearing minerals and mineralization of the Manaoke gold deposit in Nanping County, Sichuan Province. MS thesis, China University of Geosciences. 54 pp. (in Chinese with English abstract).

German, J.M., 1989. Geologic setting and genesis of gold deposits of the Dahlonega and Carroll County gold belts, Georgia. Econ. Geol. 84, 903–923.

Gu, X.X., 1988. Isotopic geology and genesis of the Dongbeizhai fine-disseminated gold deposit, Sichuan Province. MS thesis, Chengdu College of Geology. 128 pp. (in Chinese with English abstract).

Gu, X.X., 1994a. Geology, geochemistry and genesis of the Middle–Upper Triassic sedimentary rock-hosted gold deposits in NW-Sichuan, China. PhD thesis, University of Innsbruck (Austria), 247 pp.

Gu, X.X., 1994b. Geochemical characteristics of the Triassic Tethys-turbidites in northwestern Sichuan, China: implications for provenance and interpretation of the tectonic setting. Geochim. Cosmochim. Acta 58, 4615–4631.

Gu, X.X., 1994c. Mineral geochemistry and distribution of invisible gold in the Dongbeizhai sedimentary rock-hosted disseminated gold deposit, Sichuan, China: an electron microprobe study. 9th IAGOD abstracts, Beijing, pp. 792–793.

Gu, X.X., 1996. Turbidite-Hosted Micro-Disseminated Gold Deposits. Chengdu University of Science and Technology Press, Chengdu. 240 pp.

Gu, X.X., 2000. Relict sedimentary fine-laminated fabrics of stibnite and its genetic significance in the Manaoke stratabound gold deposit, Sichuan, China. J. Chengdu Univ. Technol. 27, 331–334 (in Chinese with English abstract).

Hannington, M.D., Scott, S.D., 1988. Mineralogy and geochemistry of a hydrothermal silica–sulfide–sulfate spire in the caldera of Axial Seamount, Juan de Fuca Ridge. Can. Mineral. 26, 603–626.

Hannington, M.D., Scott, S.D., 1989. Gold mineralization in volcanogenic massive sulfides: implications of data from active hydrothermal vents on the modern sea-floor. Econ. Geol. Monogr. 6, 491–507.

Hannington, M.D., Peter, J.M., Scott, S.D., 1986. Gold in sea-floor polymetallic sulfide deposits. Econ. Geol. 81, 1867–1883.

Hausen, D.M., Kerr, P.F., 1968. Fine gold occurrence at Carlin, Nevada. In: Ridge, J.D. (Ed.), Ore Deposits of the United States, 1933–1967, vol. 1. American Institute of Mining, Metallurgical, and Petroleum Engineers, New York, pp. 908–940.

Hausen, D.M., Ahlrichs, J.W., Mueller, W., Park, W.C., 1987. Particulate gold occurrences in three Carlin carbonaceous ore types. In: Hagni, R.D. (Ed.), Process Mineralogy, vol. VI. Metallurgy Society AIME, New York, pp. 193–214.

He, B.B., Gu, X.X., 2000. Evolution of the Guizhou–Guangxi Basin and mineralization of micro-disseminated gold deposits. Bull. Mineral. Petrol. Geochem. 19, 279–280 (in Chinese).

Hekinian, R., Fevrier, M., Bischoff, J.L., Picot, P., Shanks, W.C., 1980. Sulphide deposits from the East Pacific Rise, near 21 N. Science 207, 1433–1444.

Hofstra, A.H., Northrop, H.R., Rye, R.O., Landis, G.P., Birak, D.L., 1988. Origin of sedimentary rock-hosted disseminated gold deposits by fluid mixing-evidence from jasperoids in the Jerritt Canyon gold district, Nevada, USA. Geol. Soc. Aust., Abstr. 22, 284–289.

Hofstra, A.H., Leventhal, J.S., Northrop, H.R., Landis, G.P., Rye, R.O., 1991. Genesis of sedimentary rock-hosted disseminated-gold deposits by fluid mixing and sulfidization: chemical-reaction-path modeling of ore-depositional processes documented in the Jerritt Canyon district, Nevada. Geology 19, 36–40.

Holser, W.T., Kaplan, I.R., 1966. Isotope geochemistry of sedimentary sulfates. Chem. Geol. 1, 93–135.

Hu, J.P., 1991. Research on the Qiaoqiaoshang turbidite-hosted gold deposit, Sichuan Province: the characteristics of the ore-bearing turbidite and the genesis of the gold deposit. MS thesis, Chengdu College of Geology. 101 pp. (in Chinese with English abstract).

Huston, D.L., Large, R.R., 1989. A chemical model for the concentration of gold in volcanogenic massive sulfide deposits. Ore Geol. Rev. 4, 171–200.

Hutchinson, R.W., 1982. Syn-depositional hydrothermal processes and Precambrian sulphide deposits. Spec. Pap.-Geol. Assoc. Can. 25, 761–791.

Ilchik, R.P., Barton, M.D., 1997. An amagmatic origin of Carlin-type gold deposits. Econ. Geol. 92, 269–288.

Jewell, P.W., Parry, W.T., 1987. Geology and hydrothermal alteration of the Mercur gold deposit, Utah. Econ. Geol. 82, 958–1966.

Large, R.R., 1992. Australian volcanic-hosted massive sulfide de-

posits: features, styles, and genetic models. Econ. Geol. 87, 471–510.

Large, R.R., Huston, D.L., McGoldrick, P.J., Ruxton, P.A., McArthur, G., 1989. Gold distribution and genesis in Australian volcanogenic massive sulfide deposits, and their significance for gold transport models. Econ. Geol. Monogr. 6, 520–536.

Leblanc, M., Billaud, P., 1990. Zoned and recurrent deposition of Na–Mg–Fe–Si exhalites and Cu–Fe sulfides along synsedimentary faults (Bleida, Morocco). Econ. Geol. 85, 1759–1769.

Li, X.Z. (Ed.), 1989. Studies on the geologic–geochemical characteristics, metallotects, and prerequisites for ore hunting of the Dongbeizhai gold deposit in Songpan County, Sichuan Province. Unpublished report (in Chinese). 295 pp.

Li, W., Jiang, X., Ju, R., Meng, F., Zhang, S., 1989. The geological characteristics and metallogenesis of impregnated gold deposits in southwestern Guizhou, China. In: Shenyang Institute of Geology and Mineral Resources (Eds.), Contributions to the project of regional metallogenetic conditions of main gold deposit types in China, IV. Southwestern Guizhou Province. Geological Publishing House, Beijing, pp. 1–86 (in Chinese with English abstr.).

Li, X.Z., Chen, S.Y., Shen, Y.L., He, H., Jin, C., Qian, Y.Q., 1991. Studies on the metallogenic condition, metallogenic model, and prospective prediction of the Dongbeizhai-type micro-disseminated gold deposits in Songpan, Sichuan. Unpublished report (in Chinese). 143 pp.

Li, Z.Q., Chen, S.D., Li, F.C., 1994. Analysis on the metallogenic epoch of the Jinya micro-disseminated gold deposit in the western Guangxi Province. Bull. Mineral. Petrol. Geochem. 2, 77–78 (in Chinese).

Liu, J.M., 1994. Epithermal gold deposits and micro-disseminated gold deposits in China. Collective Works of Postdoctoral Station of Geology. Chengdu University of Technology, Chengdu, pp. 1–14. In Chinese.

Liu, D., Geng, W., 1985. On the mineral association and mineralization conditions of the Carlin-type gold deposits in China. Geochimica 3, 277–282.

Liu, J.S., Tao, C.G., Chen, T.J., Cheng, J.H., Chen, Y.M., 1989. On geological characteristics of three fine impregnation-type deposits in southwestern Guizhou. In: Shenyang Institute of Geology and Mineral Resources (Eds.), Contributions to the project of regional metallogenetic conditions of main gold deposit types in China, IV. Southwestern Guizhou Province. Geological Publishing House, Beijing, pp. 115–154 (in Chinese with English abstract).

Mao, S.H., 1991. Occurrence and distribution of invisible gold in a Carlin-type gold deposit in China. Am. Mineral. 76, 1964–1972.

Ohmoto, H., Rye, R.O., 1979. Isotopes of sulfur and carbon. In: Barnes, H.L. (Ed.), Geochemistry of Hydrothermal Ore Deposits, 2nd ed. Wiley, New York, pp. 509–567.

Percival, T.J., Bagby, W.C., Radtke, A.S., 1988. Physical and chemical features of precious-metal deposits hosted by sedimentary rocks in the western United States. In: Schafer, R.W., Cooper, J.J., Vikre, P.G. (Eds.), Bulk Mineable Precious Metal Deposits of the Western United States. Geological Society of Nevada, Reno, pp. 11–34.

Price, B.G., 1972. Minor elements in pyrites from the Smithers Map area, B.C. and exploration applications of minor elements studies. Unpublished Thesis, University of British Columbia. 270 pp.

Radtke, A.S., 1985. Geology of the Carlin gold deposit, Nevada. Prof. Pap.-Geol. Surv. (U.S.) 1267 (124 pp.).

Radtke, A.S., Dickson, F.W., Rytuba, J.J., 1974. Genesis of disseminated gold deposits of the Carlin-type (abstract). Geol. Soc. Amer. Bull. 6 (3), 239–240 (with Programs).

Radtke, A.S., Rye, R.O., Dickson, F.W., 1980. Geology and stable isotope studies of the Carlin gold deposit, Nevada. Econ. Geol. 75, 641–672.

Rao, R.B., Xu, J.F., Chen, Y.M., Zhou, D.B., 1987. The triassic of the Qinghai–Tibet Plateau (in Chinese). Geol. Ser. Bull. II, vol. 7. Geological Publishing House, Beijing. 239 pp.

Rona, P.A., 1984. Hydrothermal mineralization at seafloor spreading centers. Earth Sci. Rev. 20, 1–104.

Rona, P.A., Bostroim, K., Smith Jr., K.L. (Eds.), 1983. Hydrothermal Processes at Seafloor Spreading Centers. Plenum, New York. 796 pp.

Sander, B., 1970. An Introduction to the Study of Fabrics of Geological Bodies. Pergamon, Oxford. 641 pp.

Sangster, D.F., 1976. Sulphur and lead isotopes in strata-bound deposits. In: Wolf, K.H. (Ed.), Handbook of Stratabound and Stratiform Ore Deposits, vol. 2. Elsevier, Amsterdam, pp. 219–266.

Shao, J., Xu, G., Feng, S., Lu, R., Mei, J., 1982. On the study of pyrite from a certain "Carlin type" gold deposit in Shaanxi, China. Acta Petrol. Mineral. Anal. 1 (2), 25–35 (in Chinese with English abstract).

Sillitoe, R.H., Bonham Jr., H.F., 1990. Sedimentary rock-hosted gold deposits: distal products of magmatic–hydrothermal systems. Geology 18, 157–161.

Tooker, E.W. (Ed.), 1985. Geologic characteristics of sediment- and volcanic-hosted disseminated gold deposits: search for an occurrence model. U.S. Geol. Surv. Bull. 1646. 223 pp.

Turner, J.S., Gustafson, L.B., 1978. The flow of hot saline solutions from vents in the sea floor—some implications for exhalative massive sulfide and other ore deposits. Econ. Geol. 73, 1082–1100.

Wang, X.C., 1995. Riftogenesis and micro-disseminated gold deposits: Luhuo rift in E-Tethys as an example. Unpublished PhD thesis, Chengdu University of Technology. 120 pp. (in Chinese with English abstract).

Wells, J.D., Mullens, T.E., 1973. Gold-bearing arsenian pyrite determined by microprobe analysis, Cortez and Carlin gold mines, Nevada. Econ. Geol. 68, 187–201.

Xu, G., Shao, J., Feng, S., 1982a. On the mineralogical study from a "Carlin type" gold deposit in Shaanxi, China. Earth Sci. J. (J. Wuhan College Geol.) 18, 211–221 (in Chinese with English abstract).

Xu, X., Wei, Z.S., Chen, G.E., Jiao, S.R., 1982b. Sketch Table of Regional Stratigraphy of the Qianghai–Tibet Plateau. Geological Publishing House, Beijing. 163 pp., in Chinese.

Yang, S.X., 1984. A preliminary study on typomorphic characteristics of gold (in Chinese). National Symposium on Ore Mineralogy and Minerageny of China.

Zhang, M.F., Wang, Y.G., Wang, K., Luo, X.H., Wang, Z.S., 1994.

Geology of the Carlin-type gold deposits in southwestern Guizhou Province. In: Wang, Y.G., Suo, S.T., Zhang, M.F. (Eds.), Tectonics and Carlin-Type Gold Deposits in Southwestern Guizhou. Geological Publishing House, Beijing, pp. 57–84. In Chinese.

Zheng, M.H. (Ed.), 1989. An Introdution to Stratabound Gold Deposits. Press of Chengdu University of Science and Technology, Chengdu. 266 pp., in Chinese.

Zheng, M.H., Gu, X.X., Zhou, Y.F., 1990. An analysis of metallogenic physicochemical conditions and metallogenic processes of the Dongbeizhai micro-disseminated gold deposit in Sichuan Province. Miner. Depos. 9 (2), 129–140 (in Chinese with English abstract).

Zheng, M.H., Zhou, Y.F., Gu, X.X., 1991. Isotopic compositions in the Dongbeizhai fine-disseminated gold deposit, Sichuan Province, and their genetic implications. Sci. Geol. Sin. 2, 159–173.

Zheng, M.H., Liu, J.M., Schulz, O., Vavtar, F., 1993a. Schichtgebundene Goldlagerstätten in kambrishen und triassischen Gesteinen in NW-Sichuan (China). Arch. Lagerstattenforsch. Geol. Bundesanst. 15 (152 pp.).

Zheng, M.H., Gu, X.X., Zhou, Y.F., 1993b. Material source of the Dongbeizhai micro-disseminated gold deposit, Sichuan, China. Contributions to Gold Deposits of the Qinling and Daba Mountains. Geological Publishing House, Beijing, pp. 229–244.

Zheng, M.H., Zhang, B., Liu, J.M., Zhou, Y.F., Gu, X.X., Fu, R.P., 1993c. The genetic implications of the newly discovered scheelite ore bodies in the Manaoke gold deposit, Sichuan Province. J. Chengdu College Geol. 20, 1–8 (in Chinese).

Zheng, M.H., Zhou, Y.F., Liu, J.M., Gu, X.X., Liu, J.J., Zhang, B., Schulz, O., Vavtar, F., 1994. Stratabound Gold Deposits of Exhalation Type and Turbidity Type. Sichuan Publishing House of Science and Technology, Chengdu. 273 pp., in Chinese with English abstract.